The Report Committee for Hojung Jung
Certifies that this is the approved version of the following report:

Numerical Modeling for Identification of Closure Pressure from Diagnostic Fracture Injection Tests

APPROVED BY
SUPERVISING COMMITTEE:

Supervisor: _____
Mark W. McClure

Co-Supervisor: _____
Mukul M. Sharma

Numerical Modeling for Identification of Closure Pressure from Diagnostic Fracture Injection Tests

by

Hojung Jung, B.S

Report

Presented to the Faculty of the Graduate School of

The University of Texas at Austin

in Partial Fulfillment

of the Requirements

for the Degree of

Master of Science in Engineering

The University of Texas at Austin

May 2015

Dedication

To my family, Dad, Mom, and brother

Acknowledgements

First and foremost, I would like to express my deepest appreciation to my supervisor, Dr. Mark W. McClure for his great support, guidance, patience, and advice during my masters program of study. From his passion, intuition and knowledge, I have learned a lot. I would like to express deep gratitude to my co-supervisor, Dr. Mukul Sharma for his support and valuable comments. I greatly appreciate Dr. Dave Cramer as well for kindly providing the field data and sharing his input to our research.

The project is supported by the Hydraulic Fracturing and Sand Control consortium in University of Texas, Austin. I would have not been able to finish the project without the financial support of the members of the Joint Industry Project on the consortium.

I will definitely miss my kind and warm officemates Kitkwan Chiu and Yiwei Ma, research group members and the softball crews.

Abstract

History matching of Diagnostic Fracture Injection Test Field Data for Picking Closure Pressure

Hojung Jung, M.S.E

The University of Texas at Austin, 2015

Supervisors: Mark W. McClure

Mukul M. Sharma

Diagnostic fracture injection tests (DFIT) are used to estimate the magnitude of the minimum principal stress, which is assumed to be equal to fluid pressure at the moment of fracture closure. A small volume of water is injected into formation to create a fracture, the well is shut in, and eventually the fracture closes. The pressure during shut-in can be analyzed by several pressure transient methods to pick the time of fracture closure. Pressure at that time is taken to be the fracture closure pressure. In this study, DFIT simulations are performed with a fully numerical hydraulic fracturing simulator. Sensitivity analysis is done to investigate how reservoir parameters such as fracture toughness, permeability, fracture stiffness, and the magnitude of the minimum principal stress impact the DFIT pressure transient. Based on these insights, we use the simulator to match a DFIT pressure transient from a low permeability formation. We analyze the field data with conventional methods for picking closure. The simulation matches suggest

that the conventional methods can underestimate the closure pressure in low permeability formations.

Based on our results, we propose a new method for picking fracture closure based on the evolution of fracture compliance during closure. Our simulations provide insight into how the fracture compliance impacts to pressure transient. Assuming the closure pressure from our simulations matches to the data are correct, our proposed method picks the correct closure point.

This study includes simulation matches to the field data with simulations that use complicated fracture geometry, which may be realistic in some formations. The multiple fractures cases have similar pressure transients and similar reservoir parameters as the single hydraulic fracture simulations, indicating that network complexity will not necessarily be evident from the pressure transient. In the future, DFIT simulations with more complex fracture geometries will be conducted to understand how fracture geometry affects the DFIT pressure transient.

Table of Contents

List of Tables

List of Figures

Chapter 1: Introduction

1.1 Motivation and Objective

Hydraulic fracturing is an important technique for the development of unconventional resources. During hydraulic fracturing, fluid is injected at high pressure to create one or more fractures in the formation. The injection pressure must be high enough to create and propagate fractures, and so it is strongly affected by the magnitude of the minimum principal stress in the reservoir. However, the minimum principal stress cannot be measured directly. Therefore, several indirect methods exist.

One of the indirect methods is estimating closure pressure by well testing. This method assumes that the pressure when the fracture closes is equal to the minimum principal stress (Hamid, 1990). To identify the closure pressure, a fracturing test is performed, and the pressure transient during shut in period is analyzed. The diagnostic fracture injection test (DFIT) is a kind of fracturing test that is commonly conducted in shale reservoirs. In a DFIT, a small amount of water is injected and then the well is shut-in. The pressure transient after shut-in is monitored and analyzed to estimate the closure pressure of the reservoir.

For DFIT analysis, the G-function technique has been widely used. The G-function is a function of dimensionless time correlating with fluid leakoff volume that accounts for the presence of fracture propagation (Nolte, 1979). For DFIT analysis, the G-function for high fluid efficiency in low-permeability formation is used. The G-function $(G(\Delta t_D))$, an intermediate function $(g(\Delta t_D))$, and dimensionless time (Δt_D) are calculated using the following three equations.

$$G(\Delta t_D) = \frac{4}{\pi}[g(\Delta t_D) - g_0], \quad \text{(1)}$$

$$g(\Delta t_D) = \frac{4}{3}[(1+\Delta t_D)^{1.5} - \Delta t_D{}^{1.5}], \quad \text{(2)}$$

$$\Delta t_D = (t - t_P)/t_P, \quad \text{(3)}$$

where g_0 is the dimensionless loss-volume function at shut-in ($t = t_P$ or $\Delta t_D = 0$).

In the G-function technique, we plot the derivative of the pressure with respect to the natural logarithm of G-time versus G-time and pick a closure point from the plot where the derivative trend deviates from the straight line. The derivative curve facilitates identification of changes in the pressure transient at fracture closure. However, this method is based on several assumptions related to fracture shape and propagation. According to Nolte (1979), the fracture is assumed to be bi-wing and not to propagate after shut-in. However, after shut-in the fracture can keep extending (van Dam et al., 1998). Studies related to the complex geometry of fractures have been done by many researchers (Warpinski and Teufel, 1987). These complications can make picking a closure pressure from the G-function derivative plot ambiguous. Commonly, a straight line is drawn from origin to the G*dP/dG curve, and closure time is taken to be the point of deviation from linearity, such as in Figure 1.1 (a). The closure pressure is the pressure at the time of closure. However, in many field datasets, it is ambiguous where to pick the deviation from linearity (Figure 1.1 (b)).

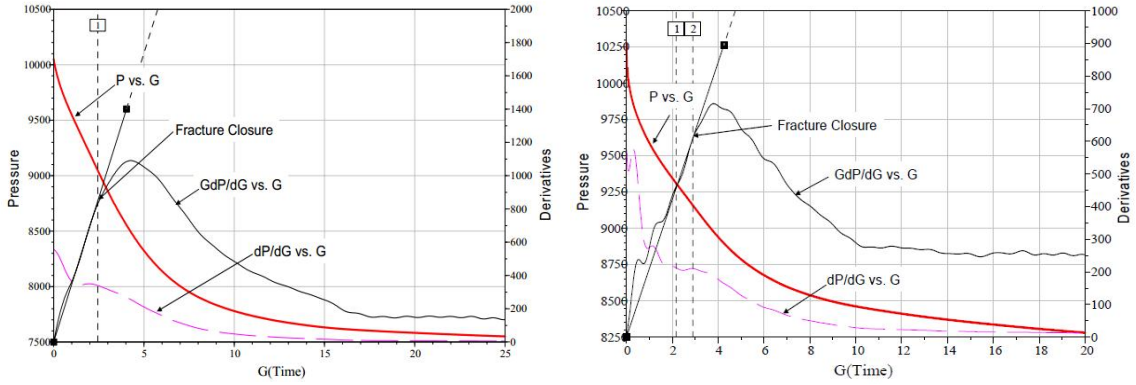

(a) Ideal G-function plot (b) Non ideal G-function plot

Figure 1.1 G-function analysis method to pick fracture closure (Figures from Barree et al., 2007)

History matching of DFIT field data has been done in this research. To match the data, it is essential to determine how fracture closure and formation properties affect the pressure transient. It is also necessary to understand how nonideal geometries can affect the results.

The main objective of this research is to improve understanding of pressure transient behavior during a DFIT. To understand how a fracture closes, DFIT simulation is done with a hydraulic fracturing simulator. The simulations are used to test whether the conventional G-function method gives the correct identification of closure pressure. The results indicate that the conventional method underestimates the minimum principal stress in low permeability rock. In response, an analysis method is presented that correctly determines closure pressure. The method is validated by history matching of field data. Simulations are also performed to investigate how complex fracture geometry affects the estimation of the minimum principal stress from DFITs.

Chapter 2: Background and Literature Review

2.1 DFIT

2.1.1 Significance of DFIT

Diagnostic fracture injection testing was developed for testing low-permeability reservoirs to determine fracture design parameters such as fracture closure pressure and pore pressure. In low-permeability reservoirs, pressure transient tests take a relatively long time because of the low rate of flow in the matrix. Therefore, conventional pressure transient tests can be impractical for low-permeability settings.

During a DFIT, a small amount of water is injected into the reservoir at low injection rate, about 1 to 5 (bbl/min), for a few minutes (Araujo et al., 2014; Cramer and Nguyen, 2013). The injected water forms fractures that propagate through the formation. After that the well is shut-in, the pressure is monitored for several days. The observed pressure data are analyzed graphically by plotting pressure versus time to estimate closure pressure, pore pressure, and the permeability of the reservoir.

2.1.2 DFIT pressure transient behavior

Figure 2.1 shows typical pressure transient behavior during a DFIT. At the beginning, the transient is dominated by fluid storage in the wellbore, and the pressure change is proportional to injection time. Wellbore storage occurs due to fluid compressibility. The wellbore storage effect coefficient is the product of wellbore volume and fluid compressibility. The pressure rises until reaching a breakdown pressure when the fracture is initiated. At the breakdown pressure, fluid begins to be injected into the fracture. After fluid goes into the fracture, the pressure decreases to the fracture propagation pressure. Pressure is relatively constant at the fracture propagation pressure

as the fracture propagates. This is because pressure increases due to fluid injection is dissipated by increasing fracture volume. At the beginning of this period, the crack created by injection is short, so fluid leakoff volume is low. However, as the fracture grows, the increased surface area of the fracture increases the fluid leakoff rate. When the well is shut-in, the pressure drops quickly to the initial shut-in pressure (ISIP) as perforation friction drop is eliminated. Eventually, the pressure decreases sufficiently that the fracture walls come into contact and the fracture closes. After fracture closure, pressure continues to decay.

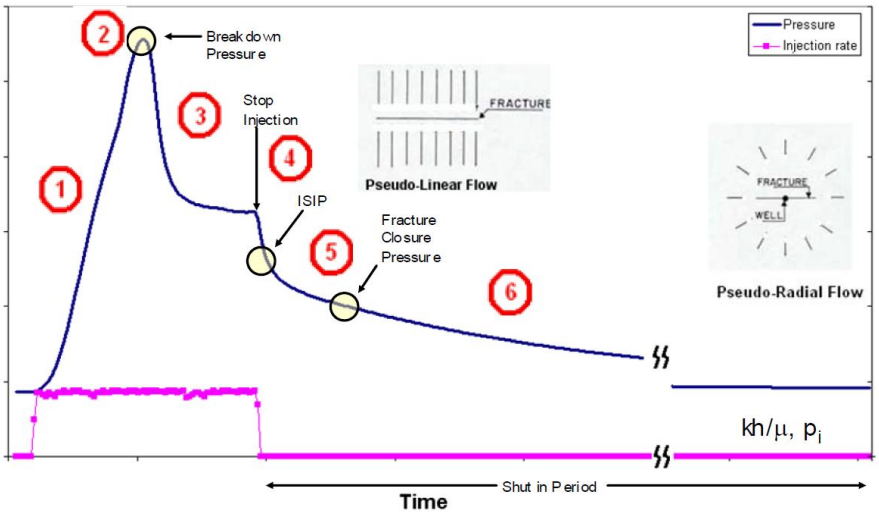

Figure 2.1 Typical DFIT pressure response (Figure from Cramer and Nguyen, 2013).

2.2 CONVENTIONAL METHODS FOR PICKING CLOSURE

To estimate the minimum principal stress from a minifrac test, several graphical analysis methods have been used: the log-log plot, square root of time plot, and G-function plot (Proskin, 1989). The G-function plot technique is an elegantly modified square-root of time plot technique (Nolte, 1979; Castillo, 1987). The square-root of time plot assumes one-dimensional leakoff along the fracture with a constant pressure

difference, whereas the G-function is modified to consider fracture propagation during the injection period.

2.2.1 Log-log diagnostic plot and square root of time plot

A log-log plot depicts pressure versus time, as shown in Figure 2.2. The log-log plot was introduced by Bourdet et al. (1989) for diagnosing flow regimes in pressure transient tests. In this technique, the pressure difference (ΔP), which is the pressure change from the beginning of the transient, is calculated. Also, the pressure derivative, (ΔP') is calculated with respect to logarithmic time such as in Equation (4).

$$\Delta P' = \frac{d(P)}{d(\ln(t))} \quad \text{...(4)}$$

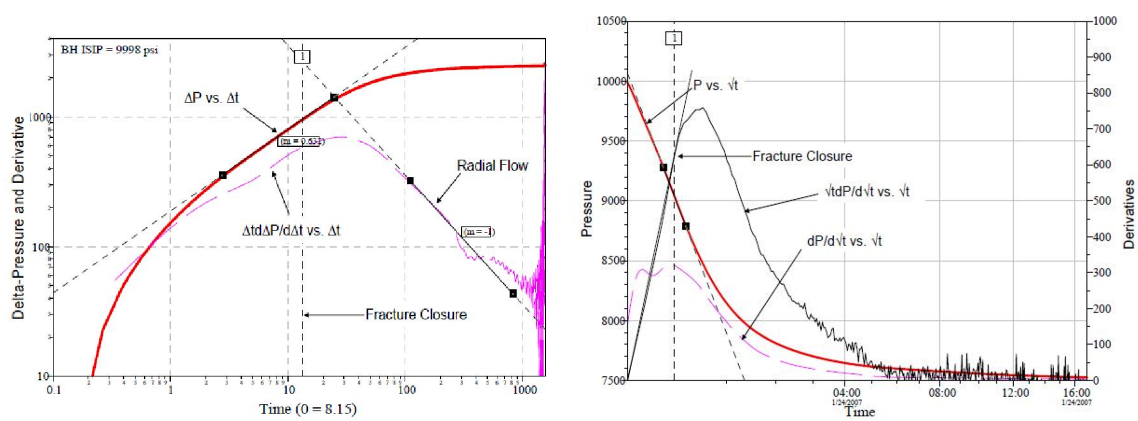

(a) Bourdet log-log plot (b) G-function plot

Figure 2.2 Comparison of plotting techniques (Figures from Barree et al., 2007).

In this plot, we can identify different flow regimes, if present, such as: wellbore storage effect with a unit slope, linear flow with a 1/2 slope, and pseudolinear flow with a -1/2 slope on log-log plot. The fracture closure is typically picked when the slope of the derivative curve changes from a 1/2 slope to a -1/2 slope.

In the square root of time plot, pressure is plotted versus the square root of time. In this plot, a straight line indicates formation linear flow. Fracture closure is assumed to occur at the end of the straight line on the square root of time plot.

2.2.2 G-function analysis

The G-function was developed by Nolte (1979). The G-function is a dimensionless function that is a transformation of the time variable as defined in Chapter 1 (Nolte, 1979). In this method, pressure and the derivative of the pressure with respect to the logarithm of G-time (G*dP/dG) are plotted versus G-time. This method has a limitation caused by assumptions that are related to fracture shape and the fluid leakoff model. According to the Nolte (1979), "*The fracture has essentially constant height, propagates through a quasi-elastic formation with negligible slip of bedding planes, was created by a constant injection rate of a power-law fluid into two symmetric wings, propagates continuously during pumping and propagation stops when pumping stops, and closes freely without significant interference from proppant*." Those assumptions are not necessarily satisfied, and it is very difficult to know the true fracture geometry.

Castillo (1987) suggests picking closure from the pressure versus G-time plot when the pressure deviates from the linear trend. However, in real field data, there can be several inflection points on the pressure versus G-time plot. Therefore, non-ideal extensions of this methodology have been researched by many authors.

Barree et al. (2007) suggests how we can overcome G-function analysis technique's limitations by explaining the graphical curve shapes with reservoir characters based on numerical simulations (Nolte, 1991). He uses G-function plots and relates non-ideal behavior to different reservoir phenomena. The base case is same as Nolte's

assumption, so the G*dP/dG curve is a straight line, and closure happens when the curve deviates from the straight line. Another case is fracture height recession or transverse fracture storage, this causes a concave upward curve in G*dP/dG. The third case is pressure-dependent leak-off. In this case the pressure G-derivative curve is concave down. The fourth case is fracture tip extension, where the fracture propagates after the well shut-in. In this case, the G-derivative curve is concave downward. Barree et al. (2007) advises not to pick closure until the G*dP/dG stops increasing.

2.3 FRACTURE CLOSURE AND FRACTURE COMPLIANCE

Fracture compliance depends on whether the fracture walls are in contact. If the walls are not in contact, the fracture is mechanically open. In this case, the compliance is relatively high and controlled by the elastic response of the surrounding rock and the fracture geometry. If the walls are in contact, the fracture is mechanically closed. The contact of the asperities in the fracture causes the compliance to be much lower, because the contact resists further compression of the fracture. The fracture retains aperture (fluid storage and conductivity) after mechanical closure because of void spaces created by roughness of the fracture walls. A fracture is mechanically closed if its fluid pressure is lower than its normal stress. "Residual aperture" (E0) is the term that we use to refer to the aperture at the moment of transition from open to closed, which occurs when fluid pressure equals the normal stress.

According to Economides and Nolte (2000), fracture width and net pressure have a linear relationship for an open fracture. This is expressed in Equation (5):

$$\bar{w} = c_f P_{net}, \quad (5)$$

where c_f is fracture compliance, $\langle \overline{w} \rangle$ is average fracture width, and P_{net} is net pressure. As long as the fracture is mechanically open and not propagating, the fracture compliance is constant. In this case, fracture compliance is a function of shear modulus, Poisson's ratio, and fracture shape. As the fracture closes, fracture compliance begins to change. Closure pressure can be picked by extrapolation of width to zero in a plot of width versus pressure plot, such as shown in Figure 2.3.

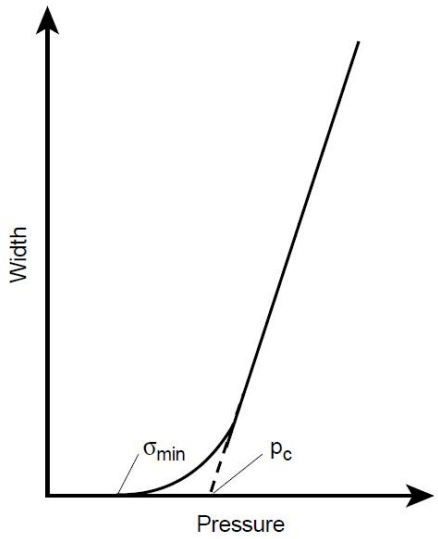

Figure 2.3 Mathematical definition of closure pressure (Figure from Economides and Nolte, 2000).

Chapter 3: Methodology

3.1 Simulation Methodology

CFRAC (Complex Fracturing ReseArch Code) is used to conduct simulations. CFRAC is a discrete fracture network simulator developed by McClure and Horne (2013). The simulator calculates pressure, deformation, sliding velocity, and direction of sliding at each element and each simulation time step. The stress induced on each element by fracture deformation is calculated. The Olson (2004) adjustment, which accounts for the finite formation height, is used to adjust the stress calculations in the psuedo-2D calculations. A fully 3D version of CFRAC is also available (McClure et al., 2015). CFRAC is briefly described in this chapter.

3.1.1 Fluid flow

The fluid is isothermal, slightly compressible liquid water with constant viscosity. Fluid flow calculations are based on the unsteady state mass balance and Darcy's law Equations, expressed in Equations (6) and (7):

$$\frac{\partial(E\rho)}{\partial t} = -\nabla\cdot(q_{flux}e) - q_{leakoff} + s \quad \text{..... (6)}$$

$$q_{flux} = -\rho\frac{k}{\mu}\nabla P \quad \text{..... (7)}$$

where E is the void aperture (the volume of fluid stored in the fracture divided by fracture surface area), t is time, q_{flux} is mass flux for the flow inside the fracture, e is hydraulic aperture (the volume divided by fracture surface area for fluid flow), s is a source term for a well, ρ is density, k is permeability, P is pressure, and $q_{leakoff}$ is leakoff rate from fracture surface area into the surrounding matrix.

Permeability and transmissivity, T, of the fracture are defined according to the following Equations (Witherspoon et al., 1980):

$$k = \frac{e^2}{12}, \quad (8)$$

$$T = ke = \frac{e^3}{12}, \quad (9)$$

The Equation for aperture depends on its loading condition. The fracture is open when the walls are out of contact because the fluid pressure has reached the normal stress on the fracture. The aperture of an open fracture is equal to E_0 plus E_{open}, the amount of mechanical separation between the fracture walls. Fractures are closed if their walls are in contact and their fluid pressure is less than their normal stress. To calculate the aperture of closed fractures, CFRAC uses a joint closure relation. This relation was developed by Barton et al. (1985) and Willis-Richards et al. (1996):

$$E = \frac{E_0}{1 + 9\sigma_n^{'} / \sigma_{n,Eref}}, \quad (10)$$

where E_0 is the void aperture when the net pressure is equal to zero, and $\sigma_{n,Eref}$ is the pressure when the void aperture closes to 90% of E_0. σ_n' is the effective normal stress, which is normal stress minus fluid pressure. In the simulations for this study, the void aperture is assumed equal to the hydraulic aperture.

Pressure, deformation, and void and hydraulic apertures are solved implicitly using the finite volume method.

3.1.2 Residual aperture of a hydraulic fracture

A key aspect of CFRAC, which is different from most other hydraulic fracturing simulators, is that is allows fractures to retain residual aperture after closure. The residual aperture is the aperture that allows fluid flow and storage in the part of fracture that has mechanical closure. In CFRAC, the fracture can be classified into two types: a hydraulic fracture and a preexisting fracture. Preexisting fracture elements exist at the beginning of the simulation. Hydraulic fractures form and propagate during the simulation.

The residual aperture at closure, E0, is the aperture at the moment of mechanical closure. A special algorithm is used to define the value of E0 at each element. The maximum value of E0 is defined to be 500 microns. However, when a new hydraulic fracture element is initiated, it has an aperture less than 500 microns. Therefore, a special treatment is needed to ensure that E0 is always less than the total aperture as the fracture is beginning to open and propagate. For each element, E0 is defined such that it is equal to the smaller of two numbers: either 500 microns or 90% of the total aperture. With this algorithm, the residual aperture increases as the crack begins to open and then reaches a maximum value. The algorithm mimics the natural process of fracture roughness generation as a crack forms for the first time. Figure 3.1 shows the fracture aperture (blue) and residual aperture at closure (red) distribution for a hydraulic fracture.

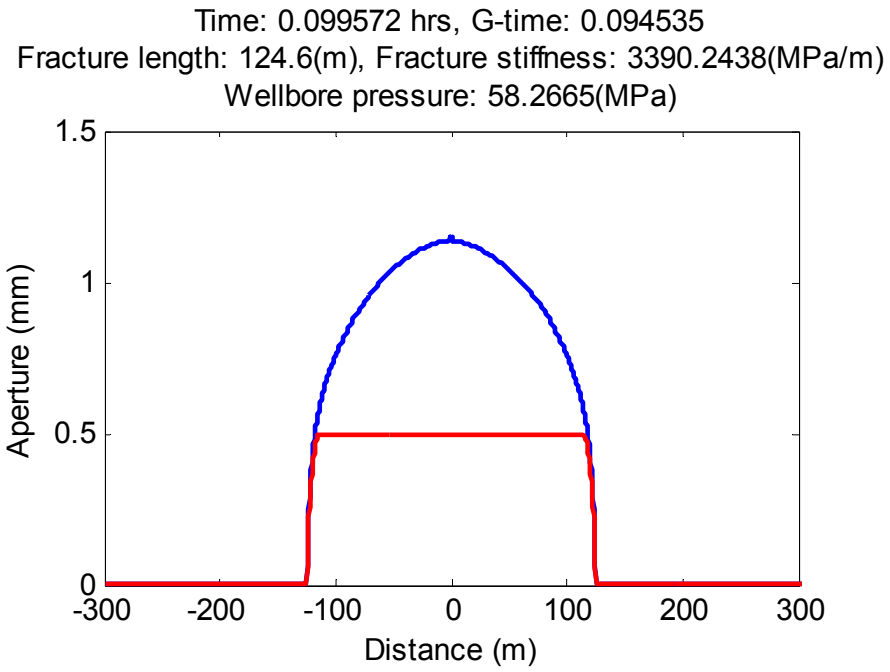

Figure 3.1 An example of residual aperture at closure (red) and aperture (blue) in CFRAC.

3.1.3 Mechanical calculations

CFRAC is a fully numerical simulator that can simulate complex fracture networks. The boundary element method is used to perform mechanical calculations, which assumes elastically homogeneous, isotropic and linear elastic deformation, and small strain. The mechanical calculations converge to analytical solutions for fracture deformation (such as Sneddon, 1946).

The normal stress applied on a fracture is calculated using Equation (11):

$$\sigma_n^r - P + \Delta\sigma_n = 0\,, \quad \text{..... (11)}$$

where σ_n^r is the normal stress and $\Delta\sigma_n$ is the change in normal stress due to backstress created by the deformation. Even after mechanical closure, CFRAC calculates the stress induced by changes in aperture. The fracture compliance, which is the derivative of aperture with respect to fluid pressure, arises from Equations (10) and (11).

3.1.4 Fracture initiation and propagation

The direction and location of newly forming hydraulic fractures must be specified in advance. For the simulations in this study, this is not a significant limitation because there is a single propagating fracture, which can reasonably be assumed to be straight. Hydraulic fracture initiation and propagation starts from wellbore and the calculation follows linear elastic fracture mechanics. The stress intensity factor (K_I) is estimated at fracture tip elements according to Equation (12), which was introduced by Olson (2007):

$$K_I = 0.806\left(\frac{2G\sqrt{\pi}}{4\left(1-v_p\right)\sqrt{a}}\right)E_{open}, \quad (12)$$

If the stress intensity factor exceeds the fracture toughness, the fracture will grow. In CFRAC, the fracture toughness is an input variable. In this study, this variable is examined to see how it changes fracture propagation and DFIT pressure transient behavior.

3.1.5 Fluid leakoff

CFRAC has two options for calculating fluid leakoff. The first is a one-dimensional fluid leakoff model, and the second is a fully numerical solution. For the 3D mode, the one-dimensional leakoff model, introduced by Vinsome and Westerveld (1980), is the only method available (McClure et al., 2015). For the 2D method, both

types of fluid leakoff are available (McClure, 2014). For simulating multiple fractures in this study, the fully numerical fluid leakoff model is used. In most simulations with only one fracture, it is acceptable to use the 1D leakoff model because the permeability is very low and the fracture is very long, so formation linear flow is dominant for the duration of the transient.

3.2 SIMULATION DESCRIPTION

To understand fracture closure, history matching of DFIT field data is conducted. To match the data, a sensitivity analysis is performed on key parameters. The field data is matched first with a model using a single fracture and then with several other possible geometries.

The field data are shown in Figure 3.2.

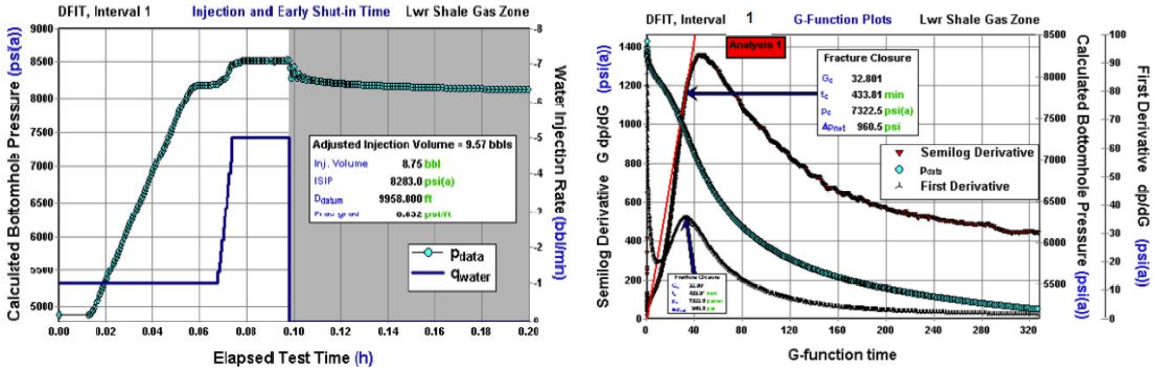

Figure 3.2 Injection rate and G-function analysis plot of DFIT field data (Figures from Cramer and Nguyen, 2013).

3.2.1 Sensitivity analysis for history matching

To match the pressure transient behavior, variables related to fracture propagation and closure can be varied. The variables are fracture toughness, permeability, fracture

stifness, and minimum principal stress. Wellbore storage is determined from a derivative of pressure with respect to injection volume at the beginning of injection.

Fracture toughness determines how far the fracture will propagate. If higher fracture toughness is used, then the fracture will propagate a shorter distance. A short fracture results in more limited area for fluid to leakoff from the fracture to the formation and reduces the rate of pressure decay after shut-in.

Permeability directly affects the rate of fluid leakoff to the formation. Higher permeability results in more rapid pressure decay after shut-in. The 90% closure stress determines how quickly fracture width reduces as fluid pressure drops. If the 90% closure stress is high, the aperture will decrease slowly (Equation (10)), indicating that the fracture is stiff. This causes the pressure derivative to jump quickly after closure.

Fractures close when their normal stress becomes greater than their fluid pressure. The minimum principal stress affects the transient by determining when fracture closure occurs.

Perforation diameter and the number of perforations are also parameters that affect pressure transient behavior. The perforation parameters determine how much the pressure decreases after shut-in due to the dissipation of the perforation friction pressure drop gradient.

3.2.2 Complicated fracture geometry

Complicated fracture geometries are studied with 2D simulations in this study. In one of the simulations, four hydraulic fracture strands are permitted to form, rather than just one (Figure 3.3). In another simulation, naturally existing transverse fractures are specified perpendicular to the propagating hydraulic fracture (Figure 3.4).

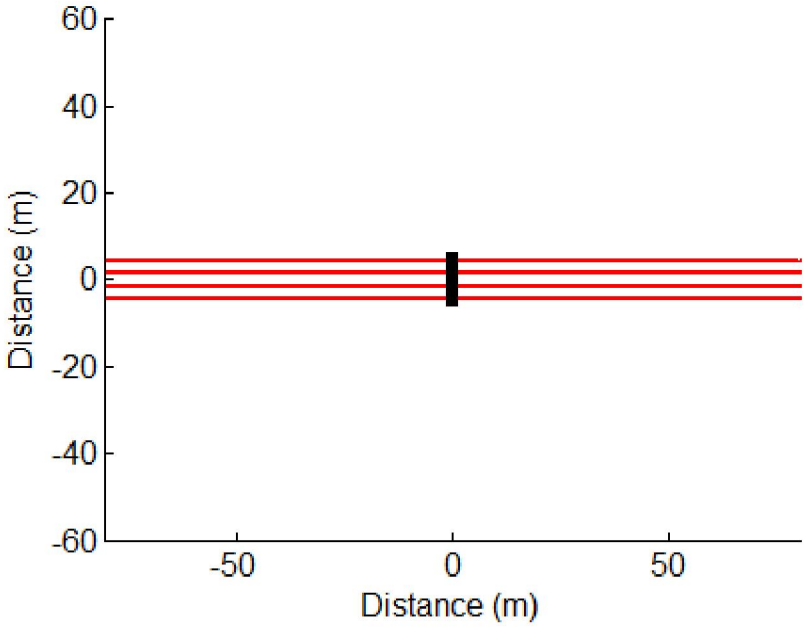

Figure 3.3 Fracture geometries of multiple strands in a fracture network.

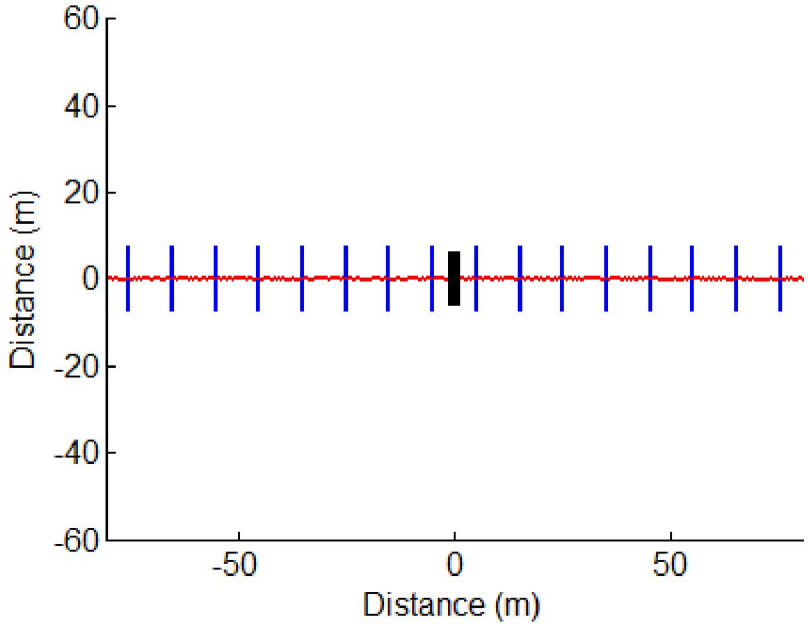

Figure 3.4 Fracture geometries of transverse fractures in a fracture network. The blue lines are natural fractures, and the red lines is hydraulic fractures.

3.3 Details of Simulation Parameters

The wellbore storage effect coefficient is 0.0184 (m^3/MPa). Fracture height is allowed to grow to a maximum of 7 m. Perforation pressure diameter is one inch, and there are 18 perforations. The injection rate was not constant over time and is shown in Figure 3.5. Initial reservoir pressure is 33.7 MPa. The simulation is continued after shut-in for about 35 days. Maximum residual aperture for the hydraulic fractures is assumed to be 500 (μm). Shear modulus (G) is fixed at 15,000 MPa and Poisson's ratio (υ) is fixed at 0.25.

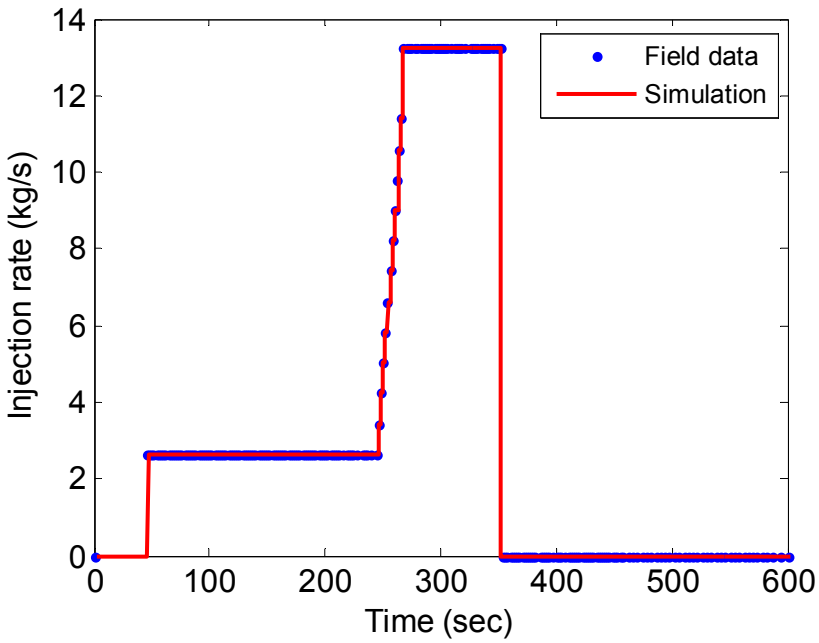

Figure 3.5 Injection rates of field data and simulation data.

3.3.1 Fracture toughness

Table 3.1 Simulation details for sensitivity to fracture toughness.

Simulation number	K1	K2	K3	K4
Fracture toughness (MPa-$m^{1/2}$)	2	4	6	8
Permeability (nD)	130			
90% closure stress (MPa)	36			
Minimum principal stress (MPa)	55.1			

3.3.2Permeability

Table 3.2 Simulation details for sensitivity to permeability.

Simulation number	P1	P2	P3	P4
Fracture toughness (MPa-$m^{1/2}$)	3.5			
Permeability (nD)	20	50	100	200
90% closure stress (MPa)	5			
Minimum principal stress (MPa)	54.5			

3.3.3 90% closure stress ($\sigma_{n,Eref}$)

Table 3.3 Simulation details for sensitivity to permeability.

Simulation number	S1	S2	S3	S4
Fracture toughness (MPa-$m^{1/2}$)	3			
Permeability (nD)	130			
90% closure stress (MPa)	5	15	25	35
Minimum principal stress (MPa)	55.1			

3.3.4 Minimum principal stress

Table 3.4 Simulation details for sensitivity to permeability.

Simulation number	M1	M2	M3	M4
Fracture toughness (MPa-$m^{1/2}$)	3.5			
Permeability (nD)	130			
90% closure stress (MPa)	5			
Minimum principal stress (MPa)	53	54	55	57

Chapter 4: Results and Discussion

4.1 SIMULATION RESULTS

4.1.1 Fracture toughness

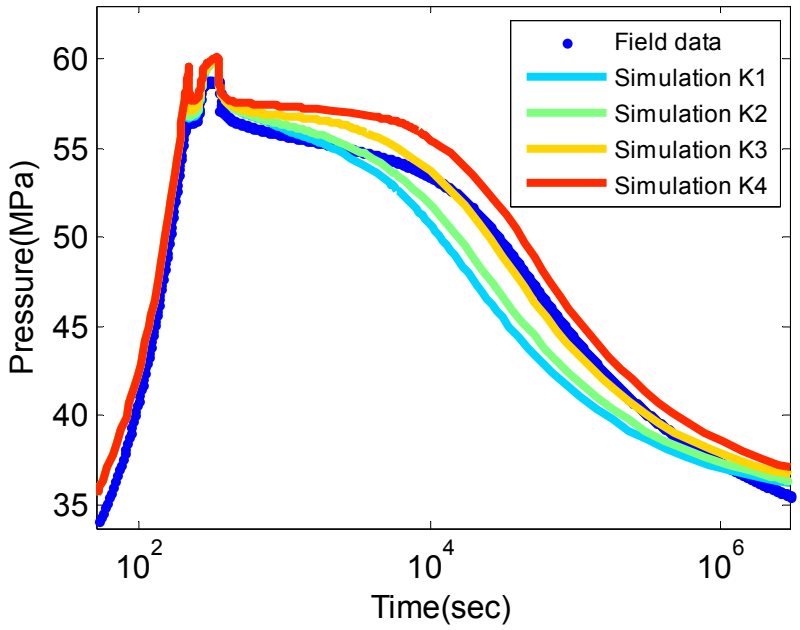

Figure 4.1 Pressure versus time graphs for different fracture toughness simulations.

Fracture toughness impacts the pressure transient behavior during both the injection and the shut-in periods. Simulation K4 has the highest fracture toughness, and the fracture propagates until the fracture half-length reaches 130 m. Right after the shut in, the length is 105 m, but the fracture tip extends further about 25 m after shut-in. For the lowest fracture toughness case, the fracture propagates an additional 90 m after shut in.

Table 4.1 Fracture half length along the fracture toughness.

Fracture toughness (MPa-$m^{1/2}$)	2	4	6	8
Final fracture half length (m)	219.4	193.8	159	129.4
Fracture half length at shut in (m)	124	123	117	109

In Figures 4.2 and 4.3, the red line indicates pressure from the field data and the blue line indicates pressure from simulation. The black line indicates the G-function derivative curve of the field data, and the green line indicates the G-function derivative curve of simulation. In the lowest fracture toughness case (Figure 4.2), an early pressure drop causes the G*dP/dG curve to rise and peak earlier than the high toughness case. The closure pressure calculated by the conventional G-function analysis method yields 49 MPa for the lowest fracture toughness case, and 52 MPa in the highest fracture toughness case. Both of the closure pressures are lower than the simulation input minimum principal stress, 55.1 MPa. In the lowest fracture toughness case, the discrepancy is higher.

According to the log-log analysis method, in the lowest fracture toughness case the closure point can be picked at 3 hours after shut in, and the closure pressure at that time is 50 MPa. In the highest fracture toughness case (Figure 4.3), the closure pressure can be picked at 15 hours after shut in, and the closure pressure at the time is 51 MPa. However, closure pressures at those picked points are lower than the input minimum principal stress. This clearly demonstrates that the traditional method of estimating closure stress underestimates the minimum principal stress, even for this simple fracture geometry.

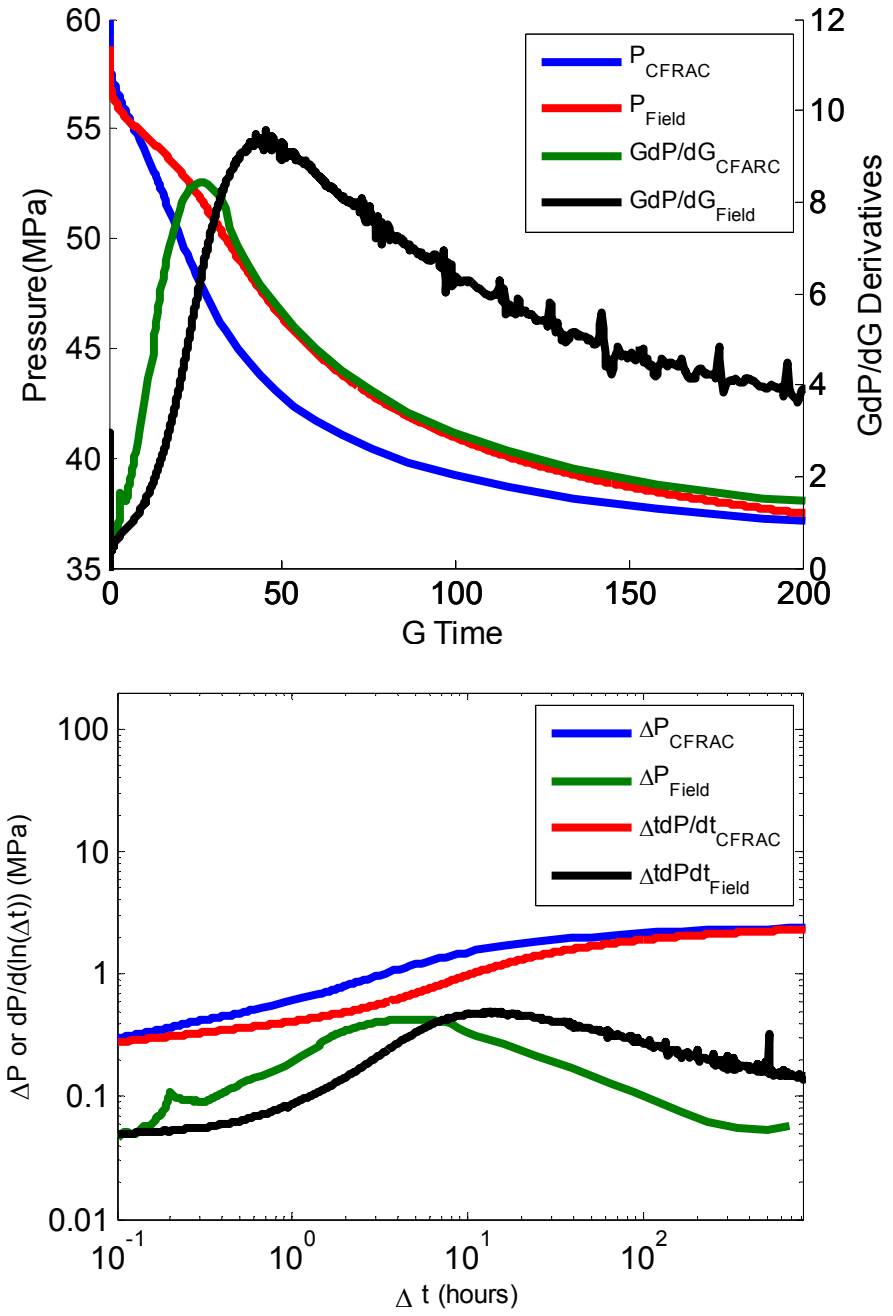

Figure 4.2 G-function analysis plot and Bourdet log-log plot for the lowest fracture toughness simulation result.

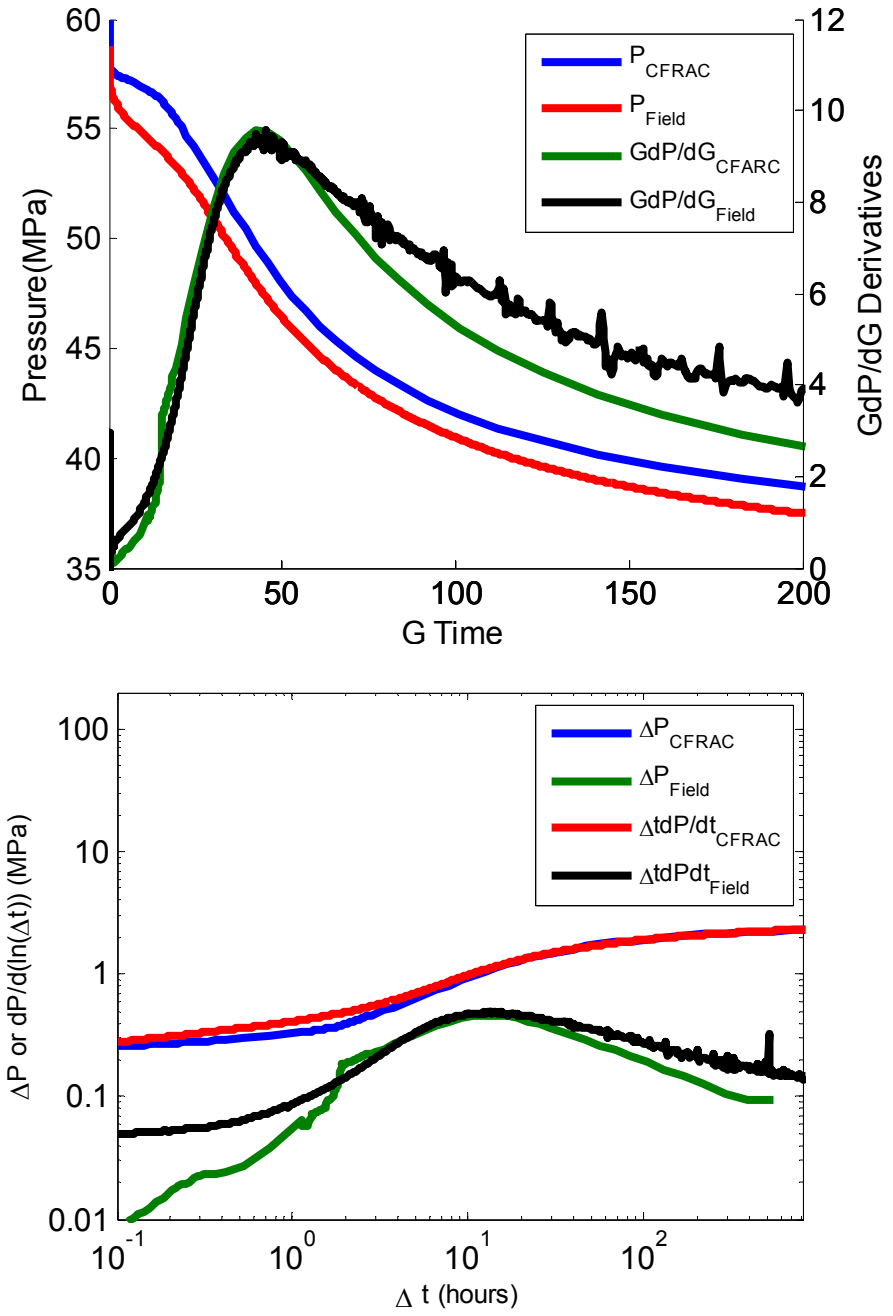

Figure 4.3 G-function analysis and Bourdet log-log analysis plot for the highest fracture toughness simulation result.

4.2.2 Permeability

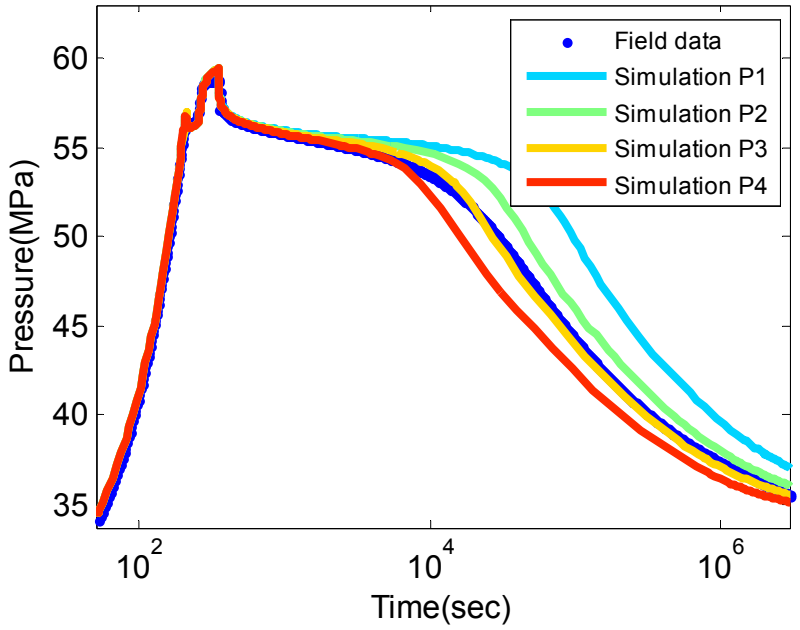

Figure 4.4 Pressure versus time graphs for different simulations in terms of permeability.

Simulation P4 has the highest permeability and the leakoff rate is highest. This causes the pressure to drop more sharply during the linear flow regime. This fast pressure drop results in a shorter fracture, so the fracture propagates until 240m in simulation P1 and until 200m in simulation P4.

Figure 4.6 shows that the G*dP/dG curve peaks much sooner in the high permeability case. The curve for the lowest permeability case goes up gradually, whereas the curve for highest permeability goes up sharply and drops sharply as well. In the low-permeability case, the closure pressure can be estimated to be 51 MPa using the conventional method. In the high permeability case, the conventional method gives an estimate of 53 MPa, which is the correct minimum principal stress in this simulation.

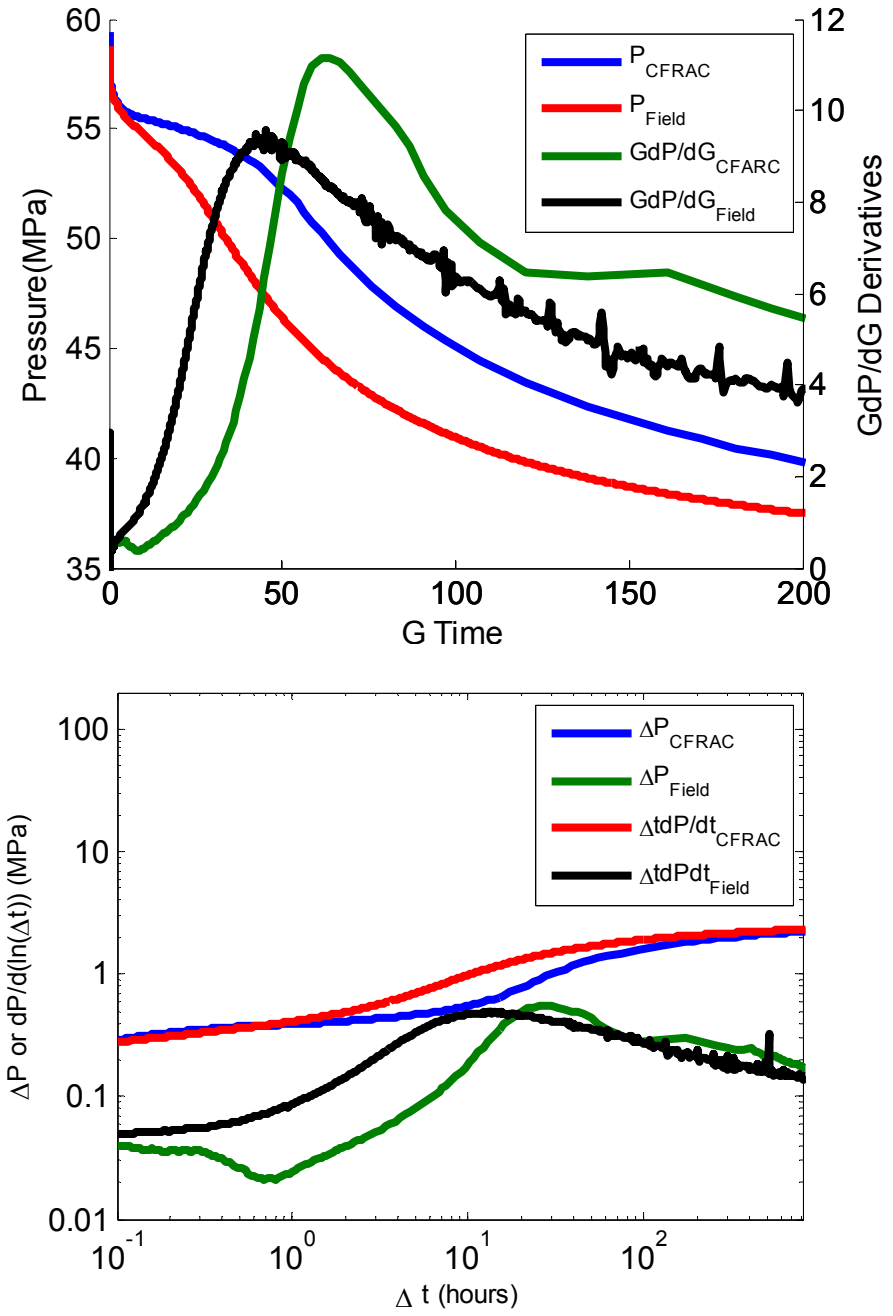

Figure 4.5 G-function analysis plot and Bourdet log-log plot for the lowest permeability simulation result.

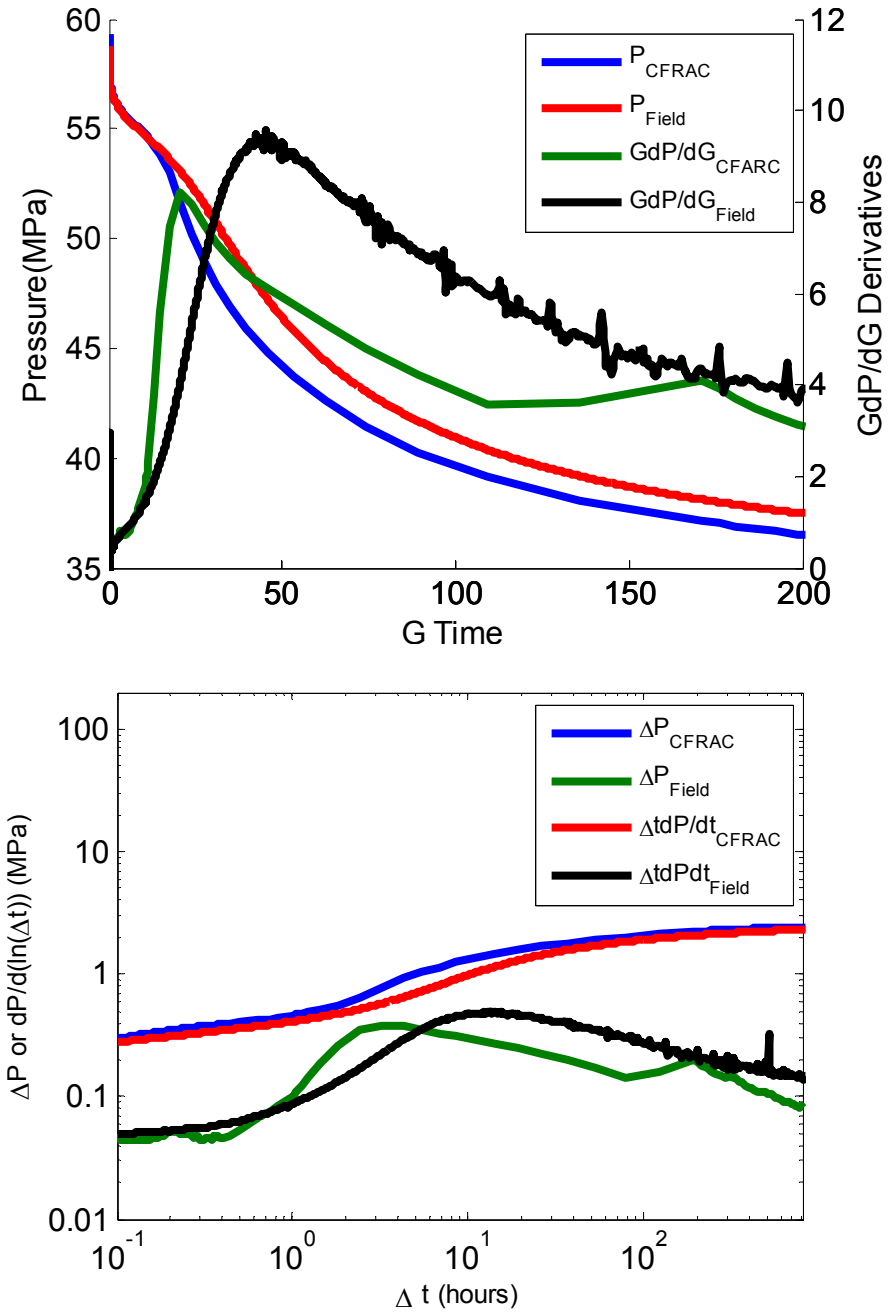

Figure 4.6 G-function analysis plot and Bourdet log-log plot for the highest permeability simulation result.

4.2.3 90% closure stress ($\sigma_{n,Eref}$)

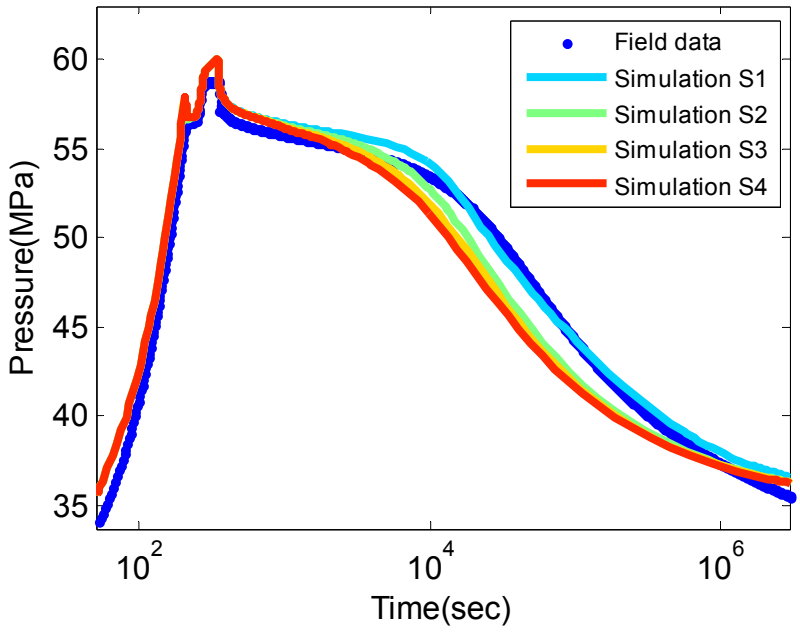

Figure 4.7 Pressure versus time graphs for different 90% closure stresses.

The 90% closure stress impacts pressure transient behavior during and after fracture closure because of the relationship between aperture and closure, as shown by Equation (10). If the 90% closure stress is low, the aperture decreases quickly after shut-in. Initially, the fracture is very compliant after closure, but with higher stress, the compliance becomes very low.

With a lower 90% closure stress, the G*dP/dG curve rises later but increases more sharply (Figure 4.8). In the lowest 90% closure stress case, the closure pressure can be estimated to be 51 MPa using the conventional method. In the highest 90% closure stress case, the conventional method can be estimated to be 50 MPa. For both cases, the conventional method gives lower closure pressure than the simulation input value (55.1 MPa).

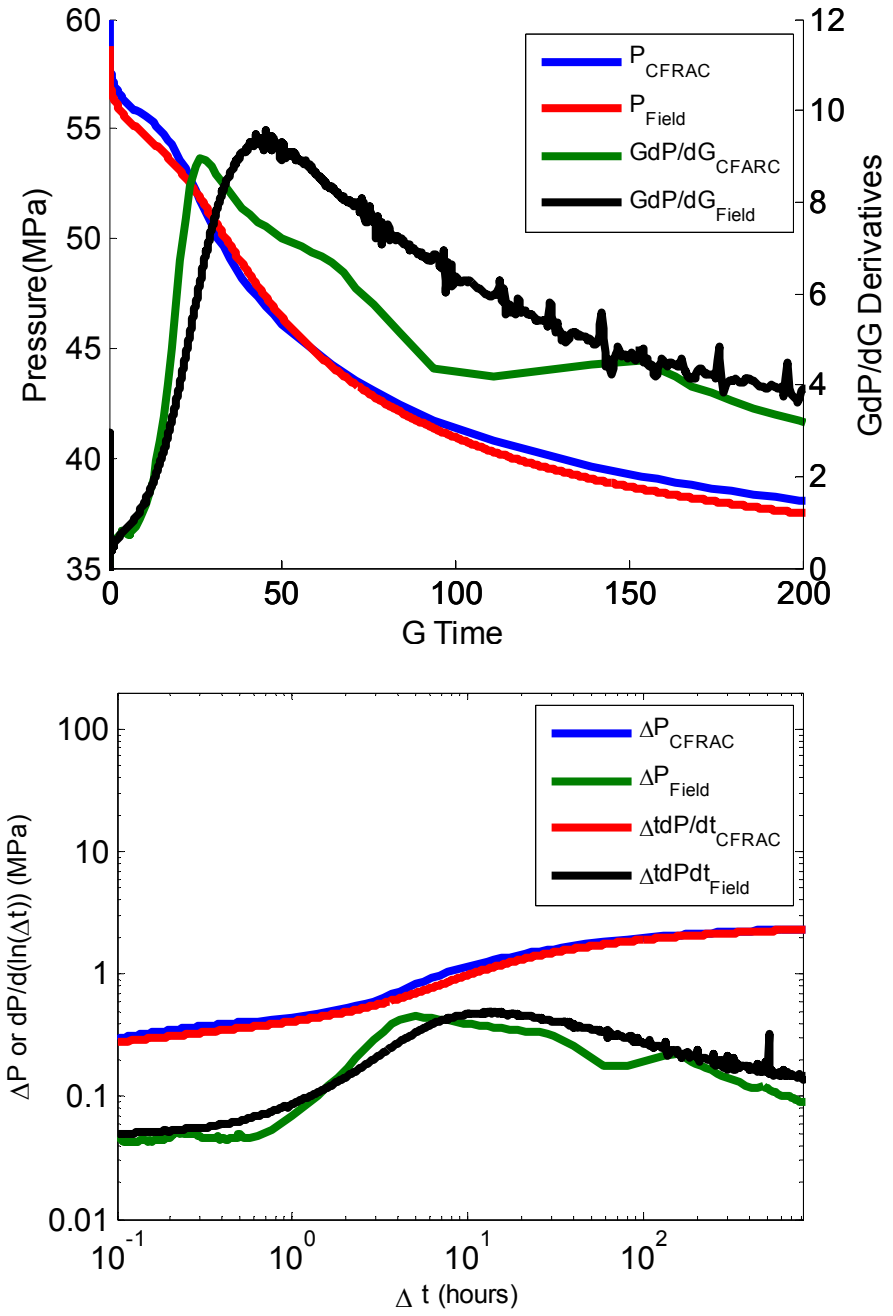

Figure 4.8 G-function analysis plot and Bourdet log-log plot for the lowest 90% closure stress simulation result.

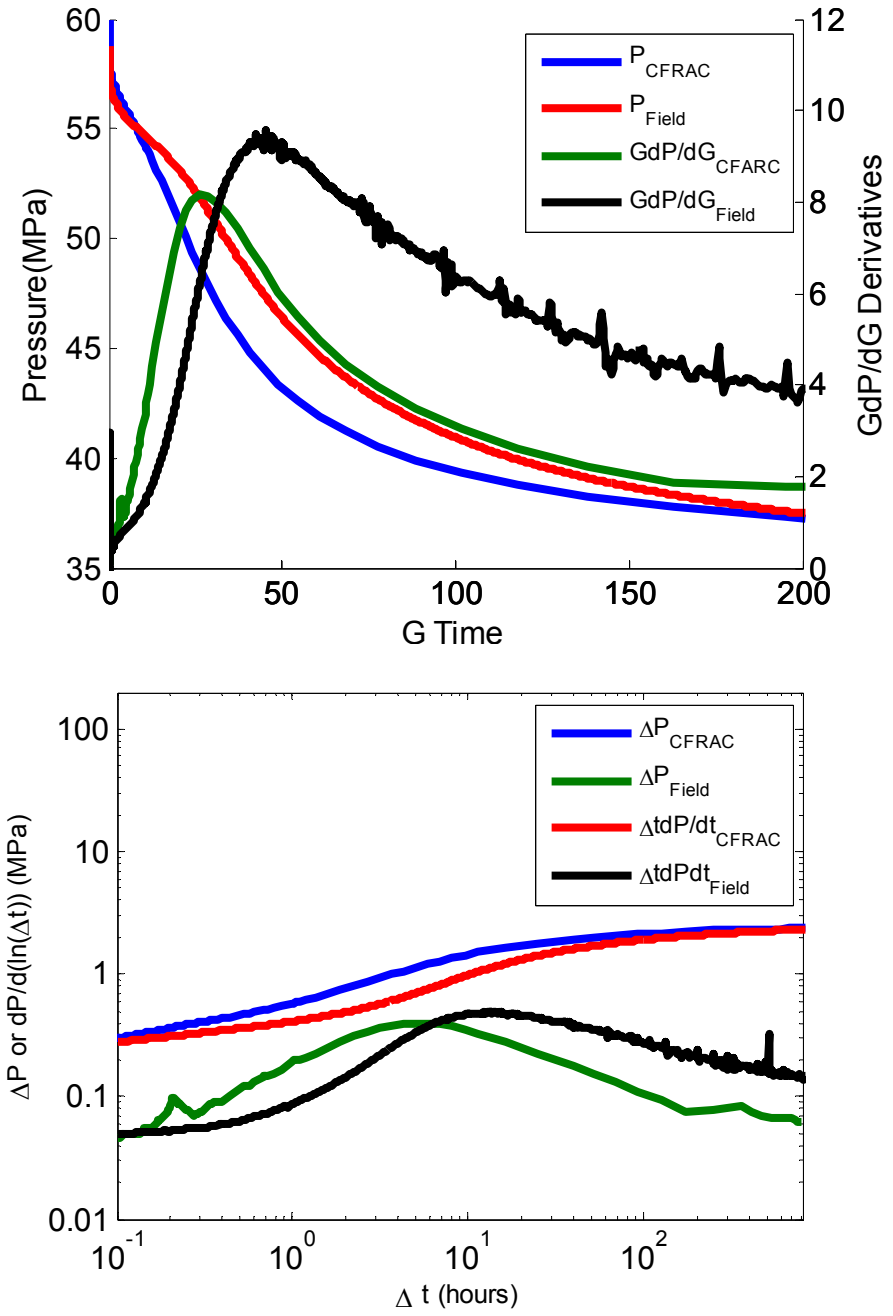

Figure 4.9 G-function analysis plot and Bourdet log-log plot for the highest 90% closure stress simulation result.

4.2.4 Minimum principal stress

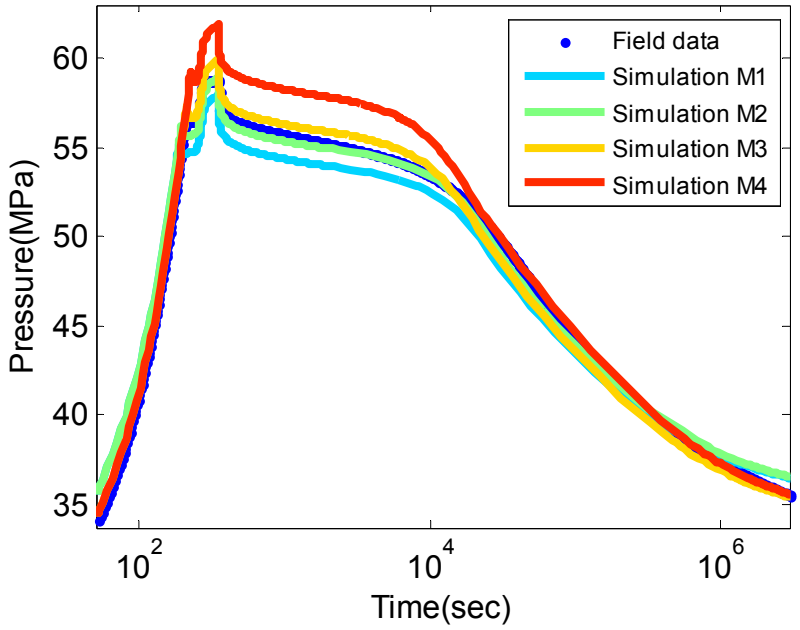

Figure 4.10 Pressure versus time graphs for different minimum principal stresses.

The minimum principal stress impacts the pressure transient behavior during all periods of the test. It primarily has the effect of translating the curve up or down. The shape of the transient is more modestly affected. It has some effect on the rate of leakoff (which affects the shape of the curve) because if minimum principal stress is increased, holding pressure constant, then the pressure difference between an open fracture and the formation increases.

As shown in Figure 4.11, because of the slower fracture closure due to low minimum principal stress, the G*dP/dG curve goes up slowly relative to the higher minimum principal stress case. In the lowest minimum principal stress case, the closure pressure is estimated as 51 MPa by the conventional method. This is still lower than the input minimum principal stress, 53 MPa. In the highest minimum principal stress case,

the conventional method gives 53 MPa, which is 4 MPa lower than input minimum principal stress. In both cases, the conventional method gives lower closure pressure.

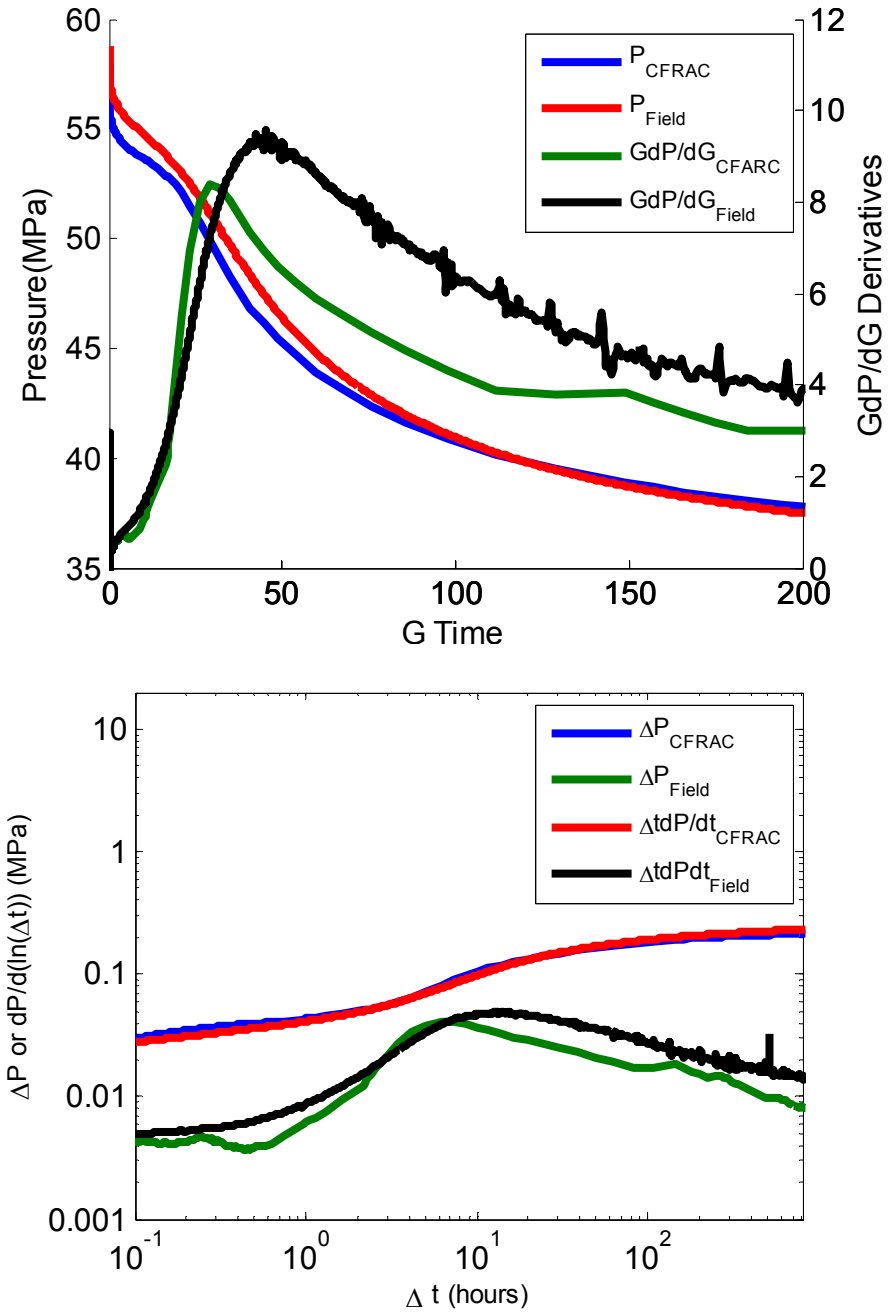

Figure 4.11 G-function analysis and Bourdet log-log analysis plot for the lowest minimum principal stress simulation results.

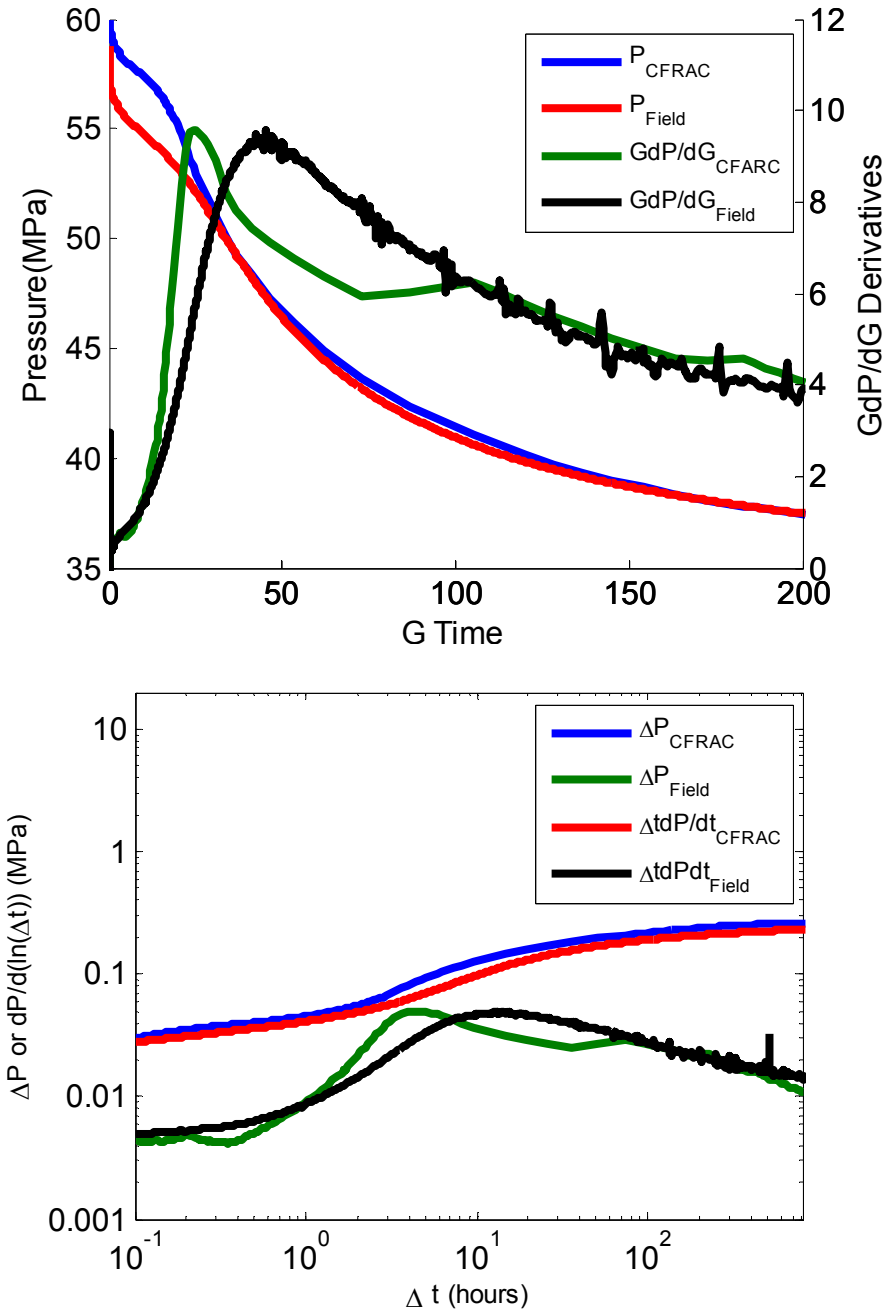

Figure 4.12 G-function analysis and Bourdet log-log analysis plot for the highest minimum principal stress simulation results.

4.2 MATCHED SIMULATION RESULT

A simulation match can be achieved to the DFIT field data from Cramer and Nguyen (2013).

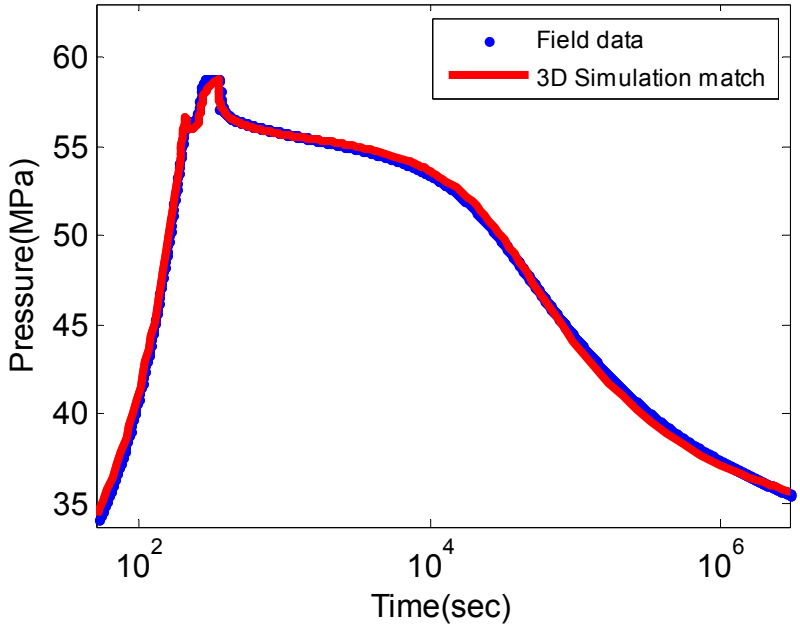

Figure 4.13 Pressure versus time graph for matched simulation result.

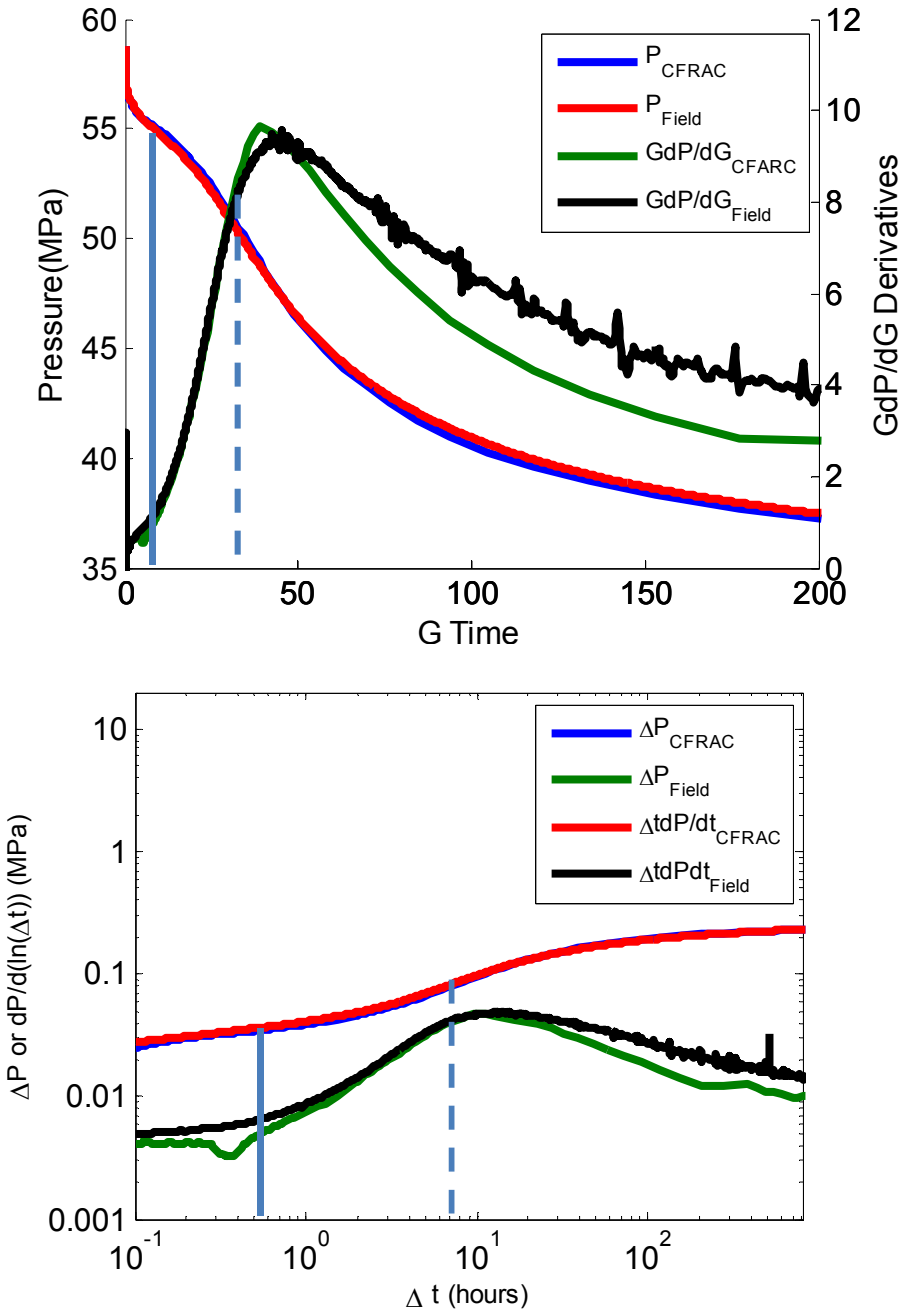

Figure 4.14 G-function analysis and Bourdet log-log analysis plots for the matched simulation result. The dashed vertical line is picked by conventional method and the solid vertical line indicates correct minimum principal stress.

Table 4.2 Matched simulation parameter values.

Fracture toughness (MPa-$m^{1/2}$)	4
Permeability (nD)	60
Minimum principal stress (MPa)	54.3
90% closure stress (MPa)	17

According to the matched simulation result, the minimum principal stress is 54.3 MPa, whereas the conventional method estimates closure pressure at 50.4 MPa (Cramer and Nguyen, 2013). Figure 4.15 shows a plot of aperture versus pressure in the fracture, taken from the simulation result. According to this figure, the minimum principal stress in our simulation should be 54.3 MPa, which is the correct value.

The difference between the correct closure pressure based on simulations and conventional methods is around 8%. This difference is magnified when we consider the net pressure, which is fluid pressure minus minimum principal stress. The initial shut in pressure is 57 MPa. Therefore, the net pressure at shut-in estimated from the conventional method is 7 MPa. However, the correct net pressure is 2.7 MPa. Therefore, this error in closure pressure leads to a huge discrepancy in net pressure.

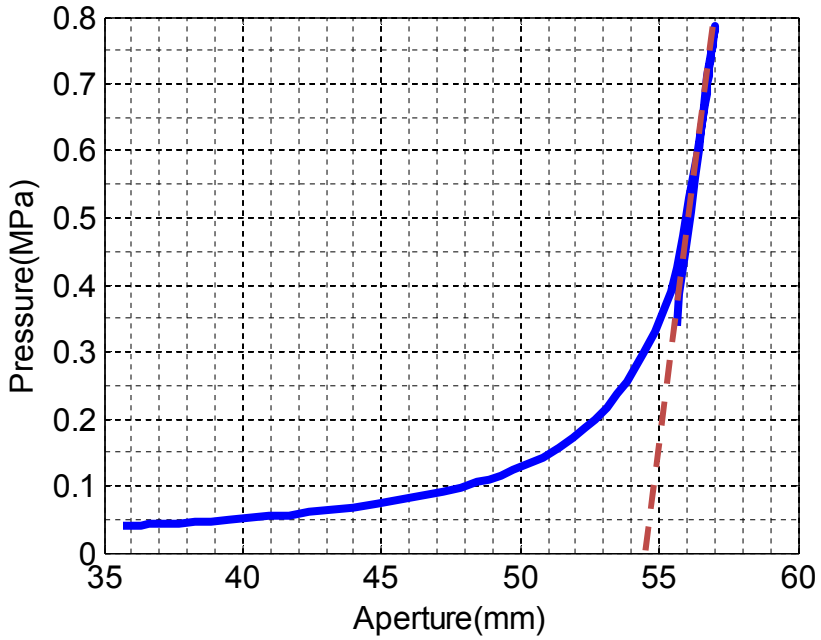

Figure 4.15 Mathematical closure pressure definition.

4.3 DISCUSSION

4.3.1 Underestimation of closure pressure by the conventional analysis method

Figures 4.16 and 4.17 show the aperture distribution along the fracture length at shut in and at the time when the fracture reaches its maximum length. In the lowest fracture toughness case, the fracture closes at around 0.32 hours (4.43 G-time). In the highest fracture toughness case, the fracture closes at around 2 hours (16.0 G-time). The distribution of aperture in Figures 4.16 and 4.17 shows that closure happens earlier than the time picked by the conventional method in Figure 4.18.

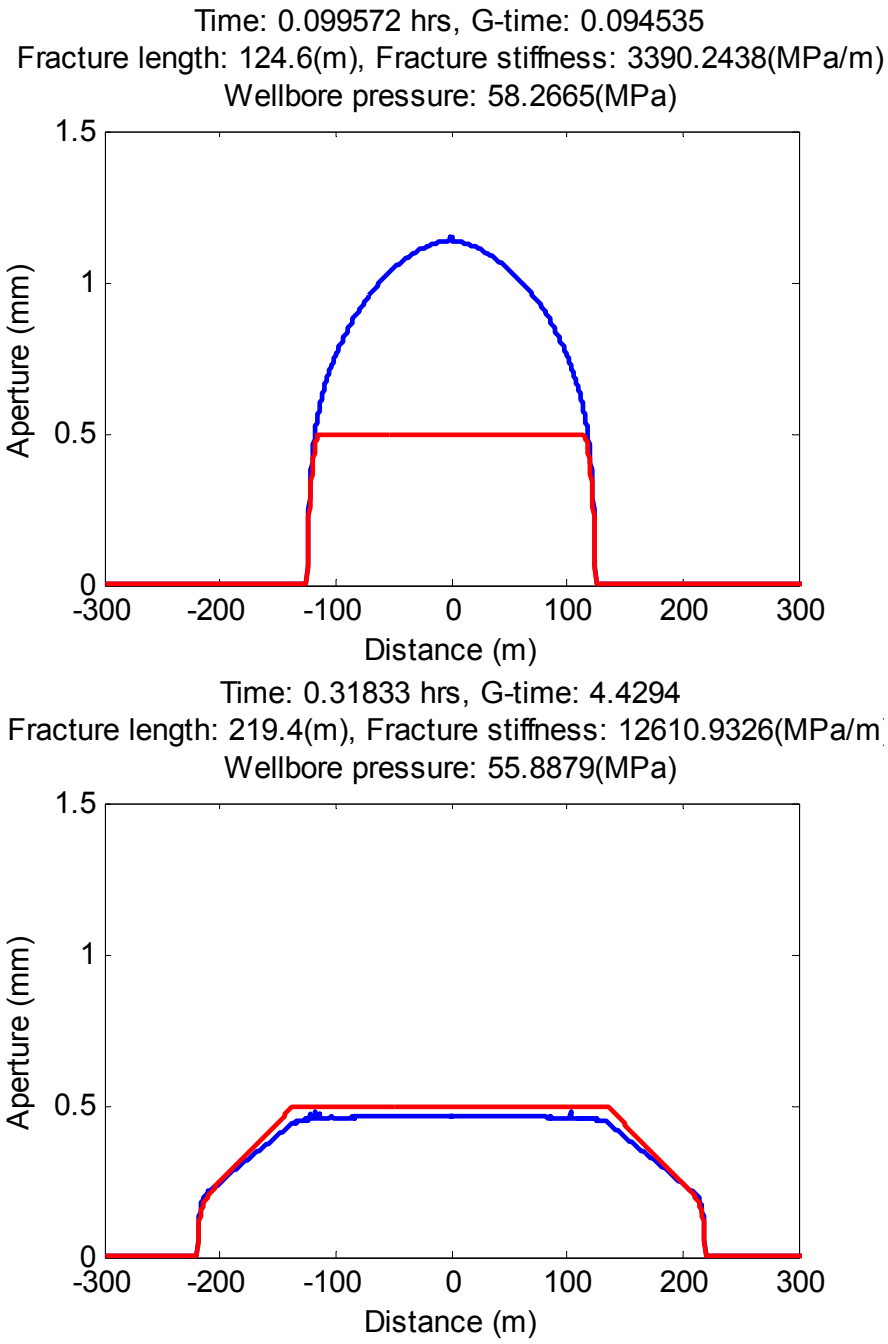

Figure 4.16 Residual aperture and aperture at shut in and at maximum length for the low fracture toughness case.

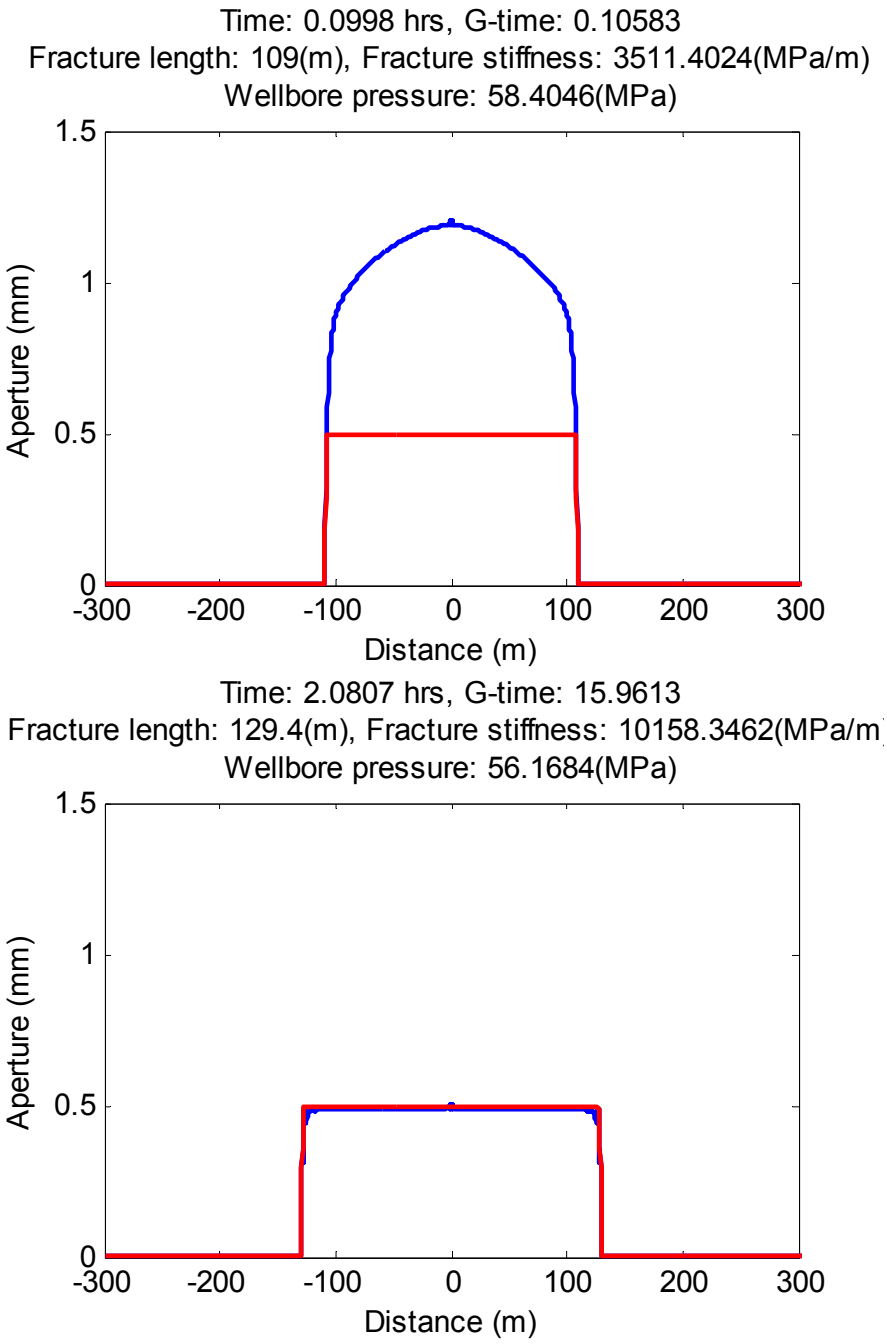

Figure 4.17 Residual aperture and aperture at shut in and at maximum length for the high fracture toughness case.

In Figures 4.18 and 4.19, the red dashed lines are the point of correct minimum principal stress (based on the simulation), and the red solid lines are closure points picked by conventional G-function analysis method. In both cases, the correct closure pressure occurs when the G*dP/dG graph starts to deviate from the linear line from origin. Right after the mechanical closure, the G*dP/dG plot goes up abruptly.

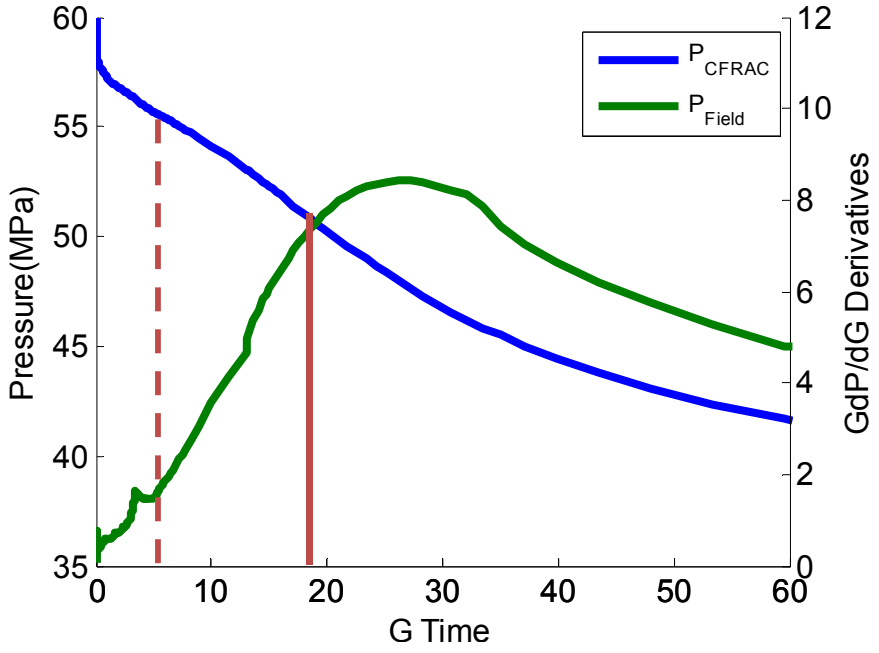

(a) Lowest fracture toughness

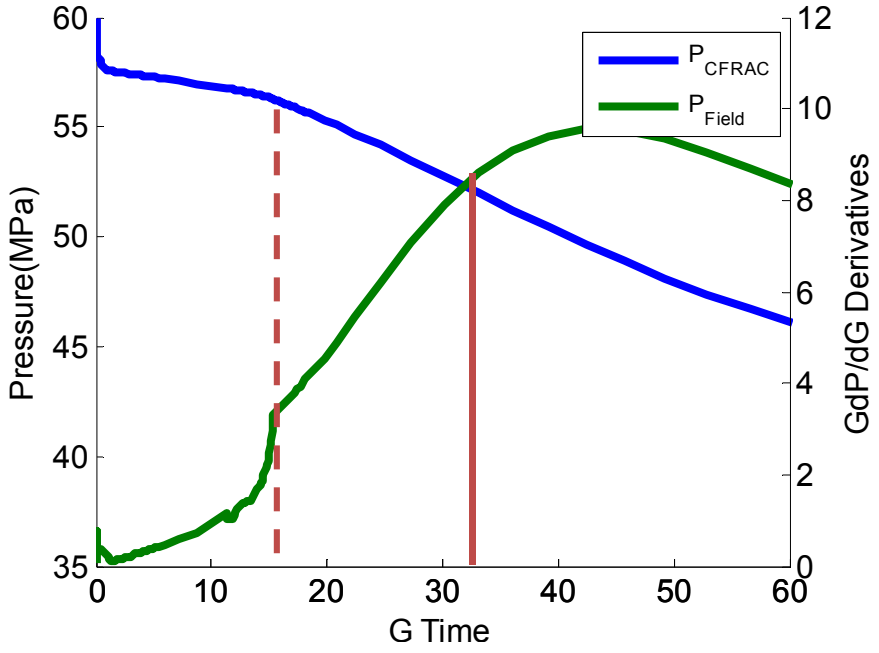

(b) Highest fracture toughness

Figure 4.18 G-function analysis for (a) the lowest and (b) the highest fracture toughness simulation results.

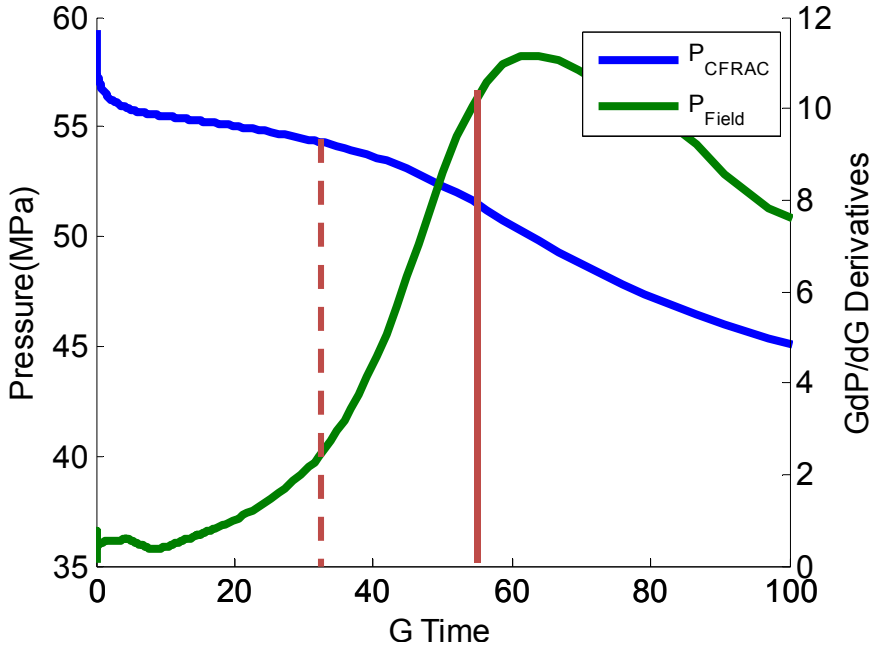

(a) Lowest permeability

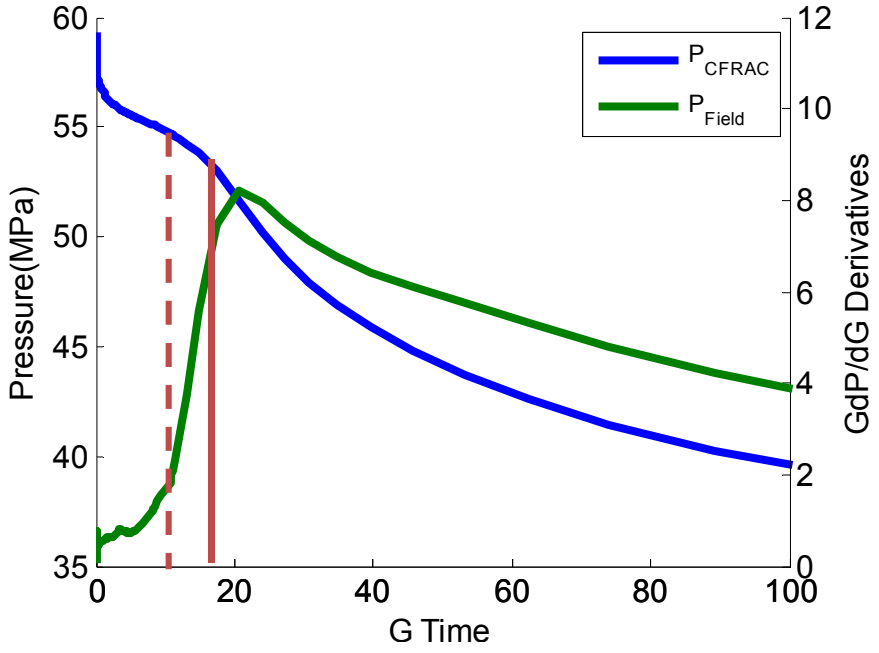

(b) Highest permeability

Figure 4.19 G-function analysis plot for (a) lowest and (b) highest permeability simulation results.

4.3.2 Fracture compliance and pressure behavior

In this section, I discuss why the G*dP/dG curve begins to sharply deviate upward after mechanical closure. Before it starts to deviate, the G*dP/dG curve is an almost straight line on the G*dP/dG versus G plot. Therefore, the slope of the G*dP/dG curve, which is equal to dP/dG, is almost constant while the fracture is open. This means that the derivative of the pressure with respect to G-time ($\frac{dP}{dG}$) is constant before the fracture closure. This derivative may be decomposed with the chain rule:

$$\frac{dP}{dG} = \frac{dP}{dV_f}\frac{dV_f}{dG}, \quad \text{.....(13)}$$

where V_f is a fracture volume and wellbore storage is neglected. The ($\frac{dP}{dV_f}$) term is proportional to the inverse of fracture compliance and proportional to the fracture stiffness. The $\left(\frac{dV_f}{dG}\right)$ term shows how much fracture volume changes with G-time, equivalent to the leakoff rate with respect to G-time.

While the fracture is open, the fracture stiffness and the leakoff rate with respect to G-time are constant. In this study, fracture height is limited to 7 m and the fracture length is relatively long relative to the fracture height, so it is similar to the PKN fracture geometry (Perkins and Kern, 1961; Nordgren, 1972). The fracture stiffness can be calculated with following relationship.

$$S_{f,PKN} = \frac{4G}{\pi(1-\nu)h_f}, \quad \text{.....(14)}$$

where G is the shear modulus, υ is Poisson's ratio, and h_f is the fracture height.

Therefore, the derivative of pressure with respect to G is constant as long as the fracture is open and the G*dP/dG curve is a straight line. Once mechanical closure occurs, the fracture stiffness increases greatly because of the additional fracture stiffness induced by fracture wall contact, and dP/dG increases significantly.

The fracture compliance can be calculated directly from the simulation results by using the derivative of average fracture aperture with respect to average fracture pressure. In Figure 4.20, the fracture stiffness and compliance are given as a function of time from the highest fracture toughness simulation. Prior to closure, the fracture stiffness is nearly constant. The calculated theoretical fracture stiffness is 3.6 (MPa/mm), equal to the stiffness shown in Figure 4.20. At the moment of mechanical closure, the fracture compliance starts to significantly drop, and the stiffness starts to increase. As a result, the derivative of the pressure with respect to G begins to increase at this point, yielding an indication of fracture closure.

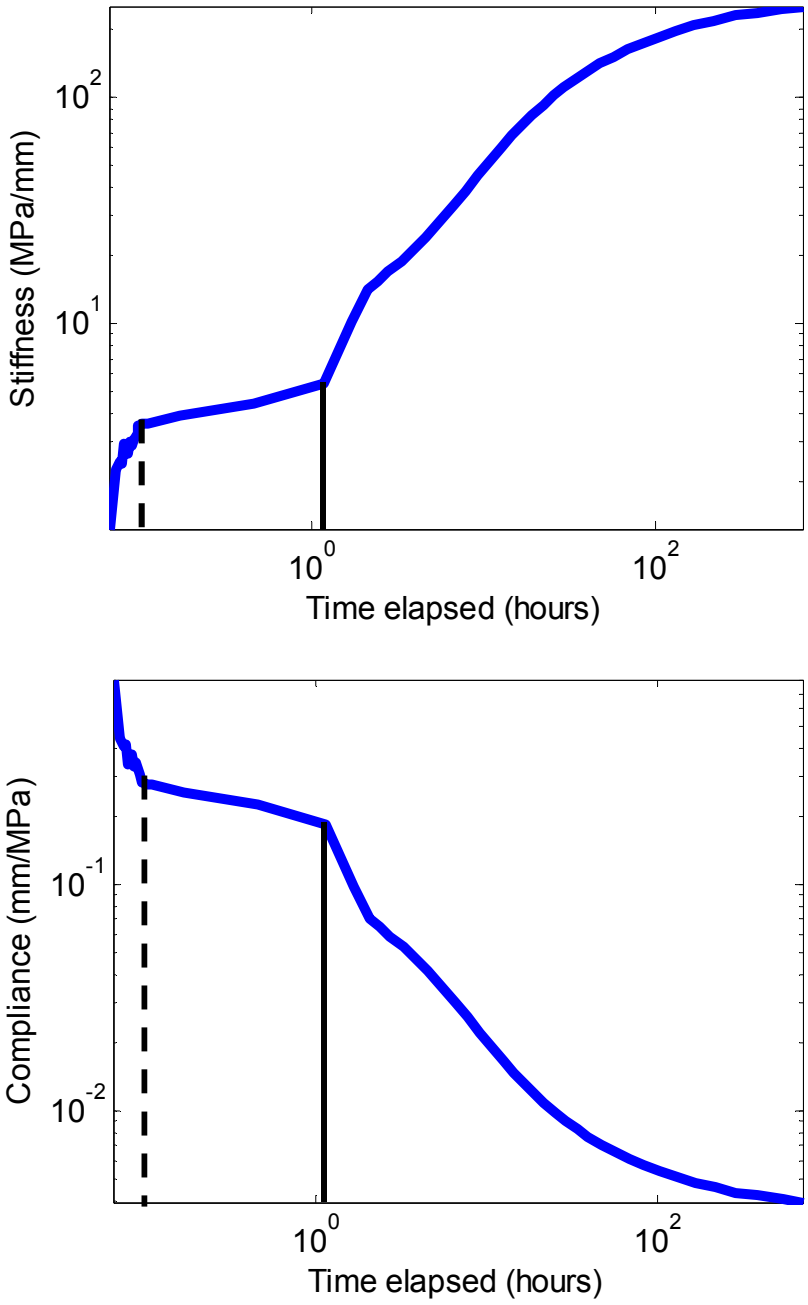

Figure 4.20 Effective fracture stiffness and compliance along the time elapsed. The dashed vertical line shows when the height recession occurs, and the solid vertical line represents at the moment of the mechanical closure.

4.3.3 Proposed method to pick the closure point

Because of the evolution of fracture compliance during closure, it can be concluded that closure can be picked when the G*dP/dG curve begins to sharply deviate upward from its initial straight line trend. Figure 4.21 is a G-function analysis plot of the field data, showing both the conventional method and the method proposed in this study. Our proposed method picks closure pressure at 55 MP which is close to the minimum principal stress inferred from the simulation match.

Figure 4.22 show the distribution of the aperture along the fracture length during the simulation that matches the field data. We can check to see when mechanical closure occurs by looking directly at the simulation result. The result confirms that mechanical closure happens at the point when G-time equals 5.6 hours and time equals 0.42 hours after shut in. As shown in Figure 4.22, this is the moment the fracture compliance begins to decrease significantly in the simulation.

The Figure 4.23 shows the distribution of the aperture at the vertical cross section of the fracture. A modest amount of fracture height recession occurs. The fracture actually closes inward from the top and bottom, and this closure process begins prior to full closure. However, the sharp drop in compliance does not occur until the fracture has fully closed.

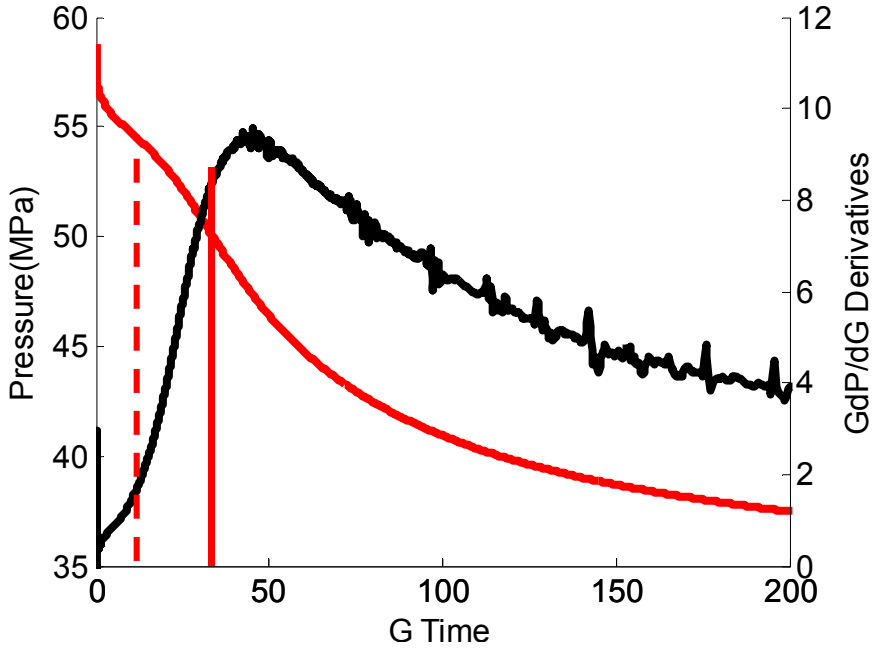

Figure 4.21 G-function analysis method from a field dataset.

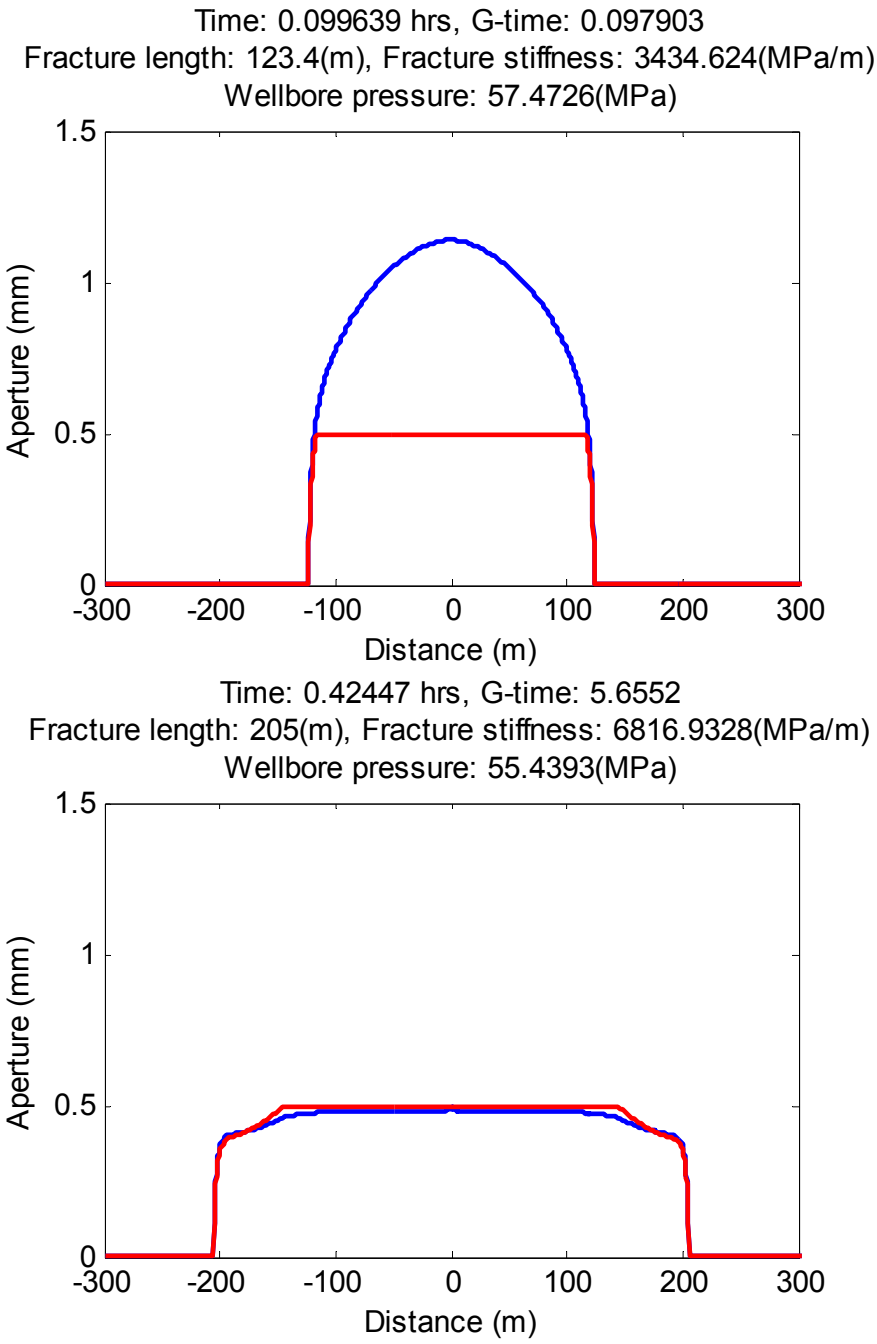

Figure 4.22 Distribution of the aperture at shut in and at the fracture propagation stop along fracture length and height. Red line represents residual aperture and blue line is aperture.

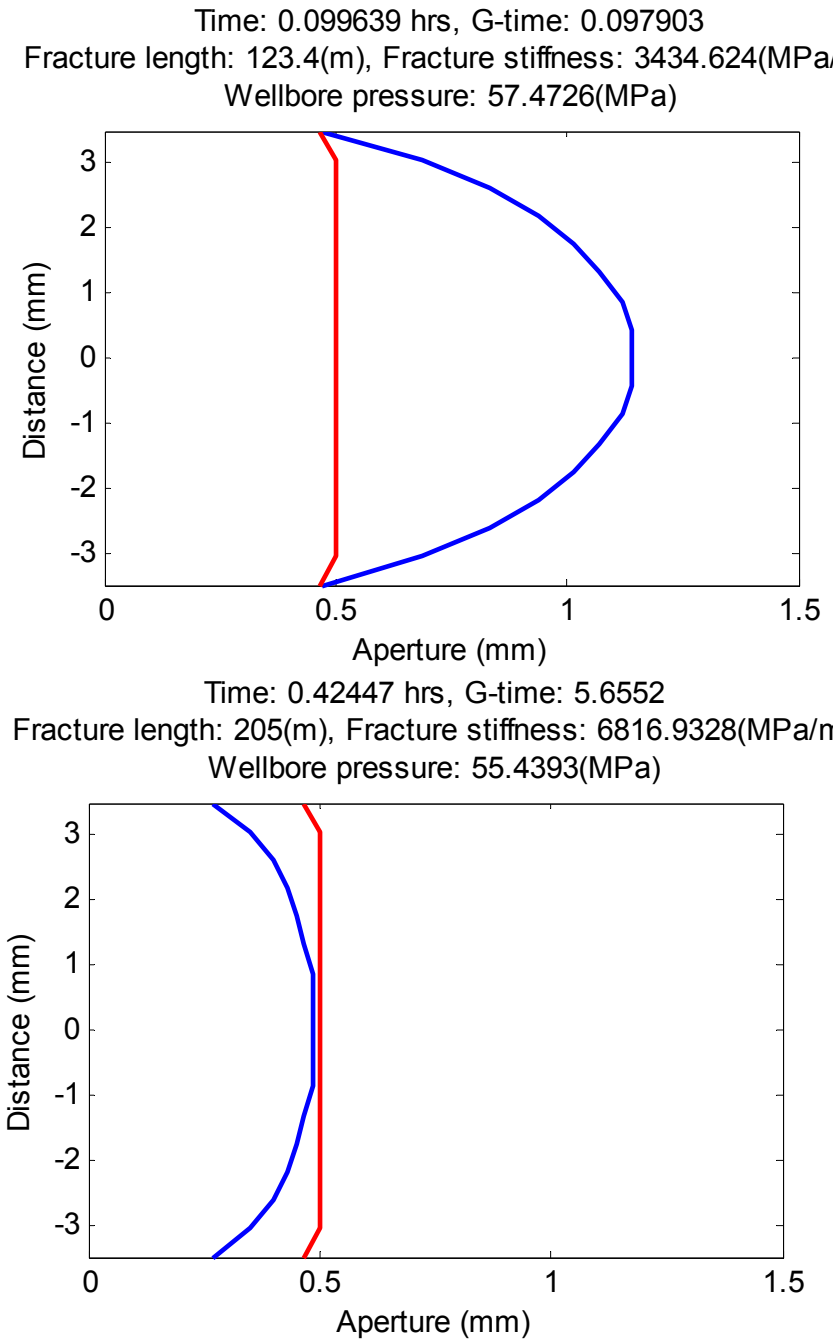

Figure 4.23 Distribution of the aperture at shut in and at the fracture propagation stop along fracture length and height. Red line represents residual aperture and blue line is aperture.

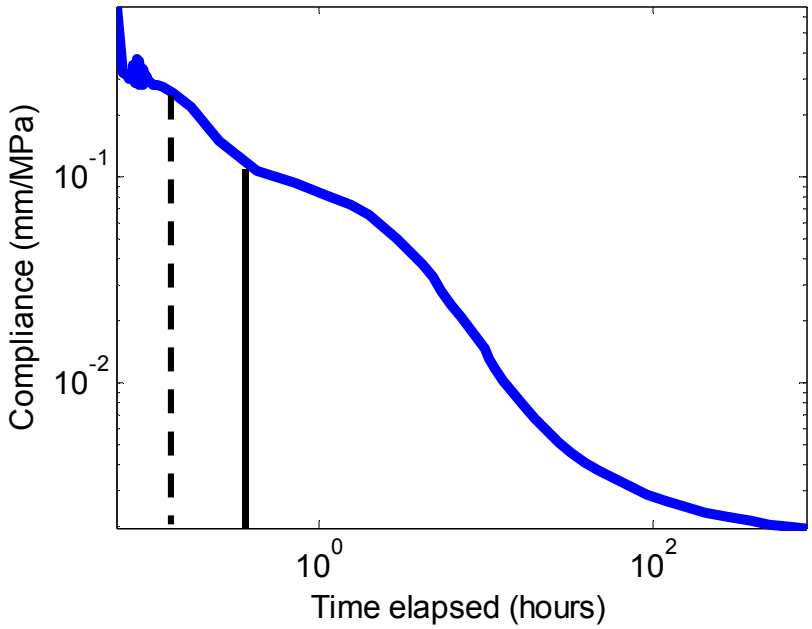

Figure 4.24 Effective fracture compliance along the time elapsed. The dashed line represents at the beginning of the height recession, the second dashed vertical line represents at the moment of full mechanical closure along the length.

4.3.4 Multiple Fractures

The simulation match to the field data predicts a long fracture with half-length of 205 m. This may seem somewhat unrealistic because the injection volume is small. In this section, we consider the possibility that rather than one single fracture, there are multiple strands or transverse fractures connected to a single hydraulic fracture. Using this fracture geometry and by changing the input variables, history matching for the field data can be performed. The simulations in this section are done with the 2D (pseudo-3D) version of CFRAC.

4.3.4.1 2D Matched Base Case

To compare how different fracture geometry changes the pressure transient, the DFIT field data is matched with a single hydraulic fracture; the match is very similar to results from the field data. The simulation parameters are very similar, but not identical, to the parameters from the match with the 3D simulator.

Table 4.3 Simulation match input variables for a single hydraulic fracture geometry.

Fracture toughness (MPa-m$^{1/2)}$	2
Permeability (nD)	50
Minimum principal stress (MPa)	55.1
90% closure stress (MPa)	45

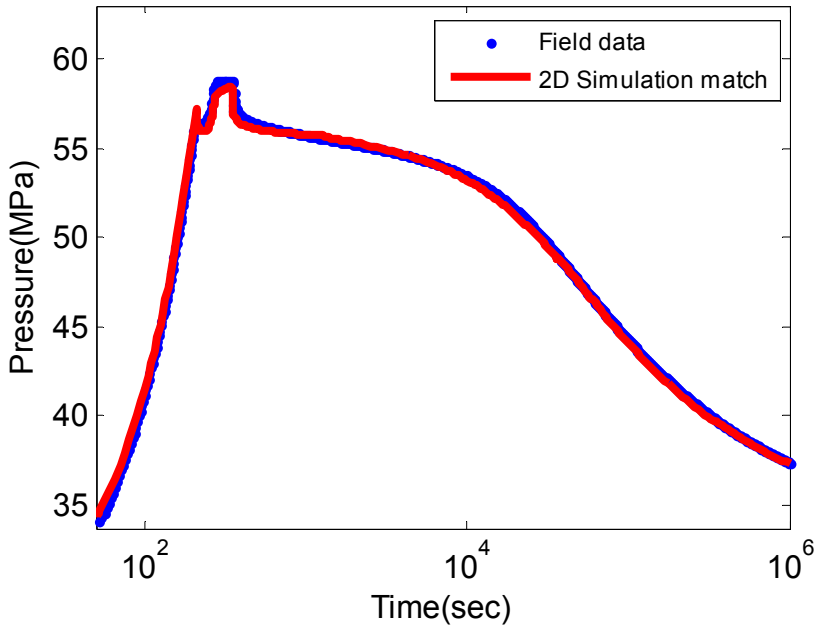

Figure 4.25 Simulation match with single hydraulic fracture geometry.

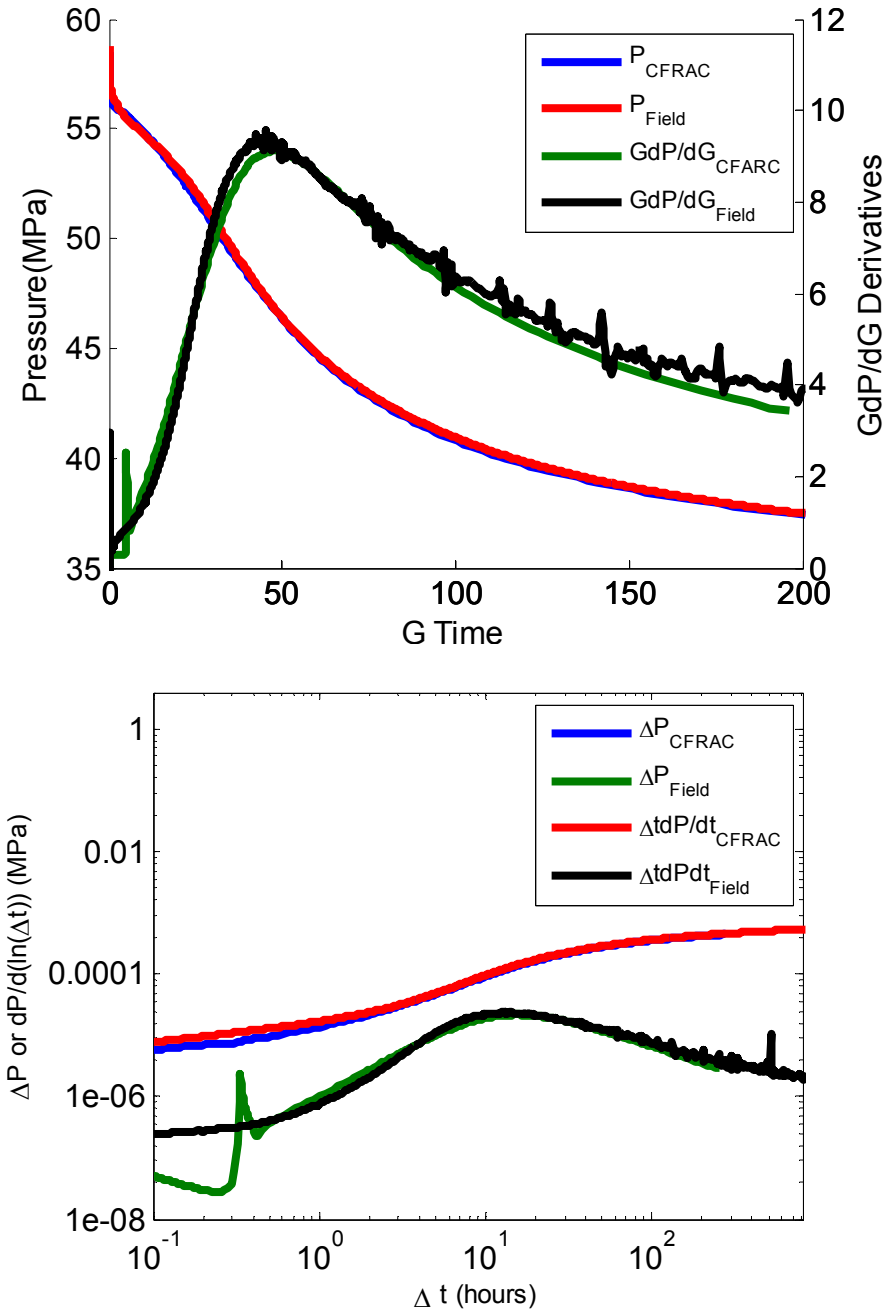

Figure 4.26 G-function analysis and Bourdet log-log analysis plots of 2D simulation match.

4.3.4.2 Multiple strands of hydraulic fractures

With multiple hydraulic fracture strands, there is more fracture surface area and leakoff occurs more rapidly. Therefore, fracture toughness must be increased relative to the basecase. The fracture geometry of the simulation match is shown in Figure 4.29. The length is significantly reduced with multiple strands of hydraulic fractures.

Table 4.4 Simulation match input variables for four strands hydraulic fractures geometry.

Fracture toughness (MPa-m$^{1/2)}$	4
Permeability (nD)	50
Minimum principal stress (MPa)	55.1
90% closure stress (MPa)	50

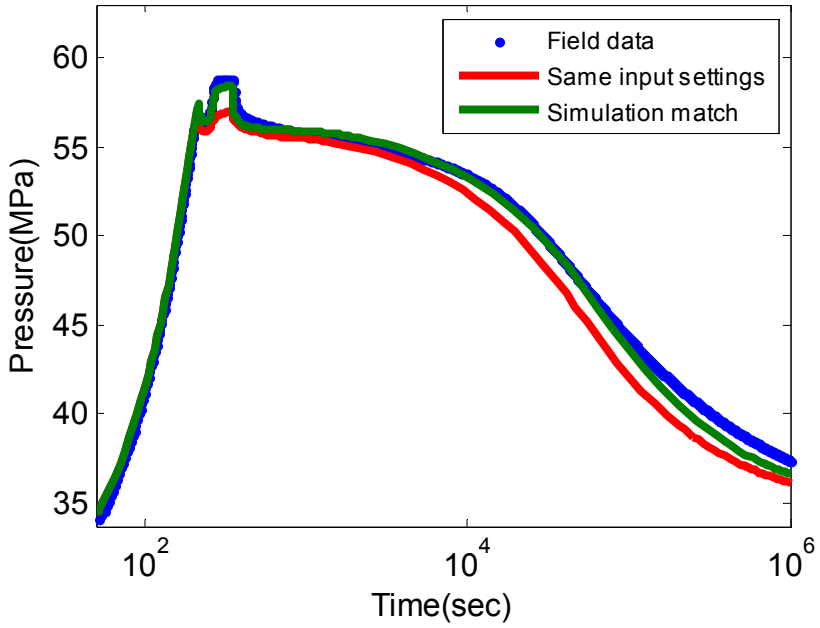

Figure 4.27 Simulation results with four strands of hydraulic fractures.

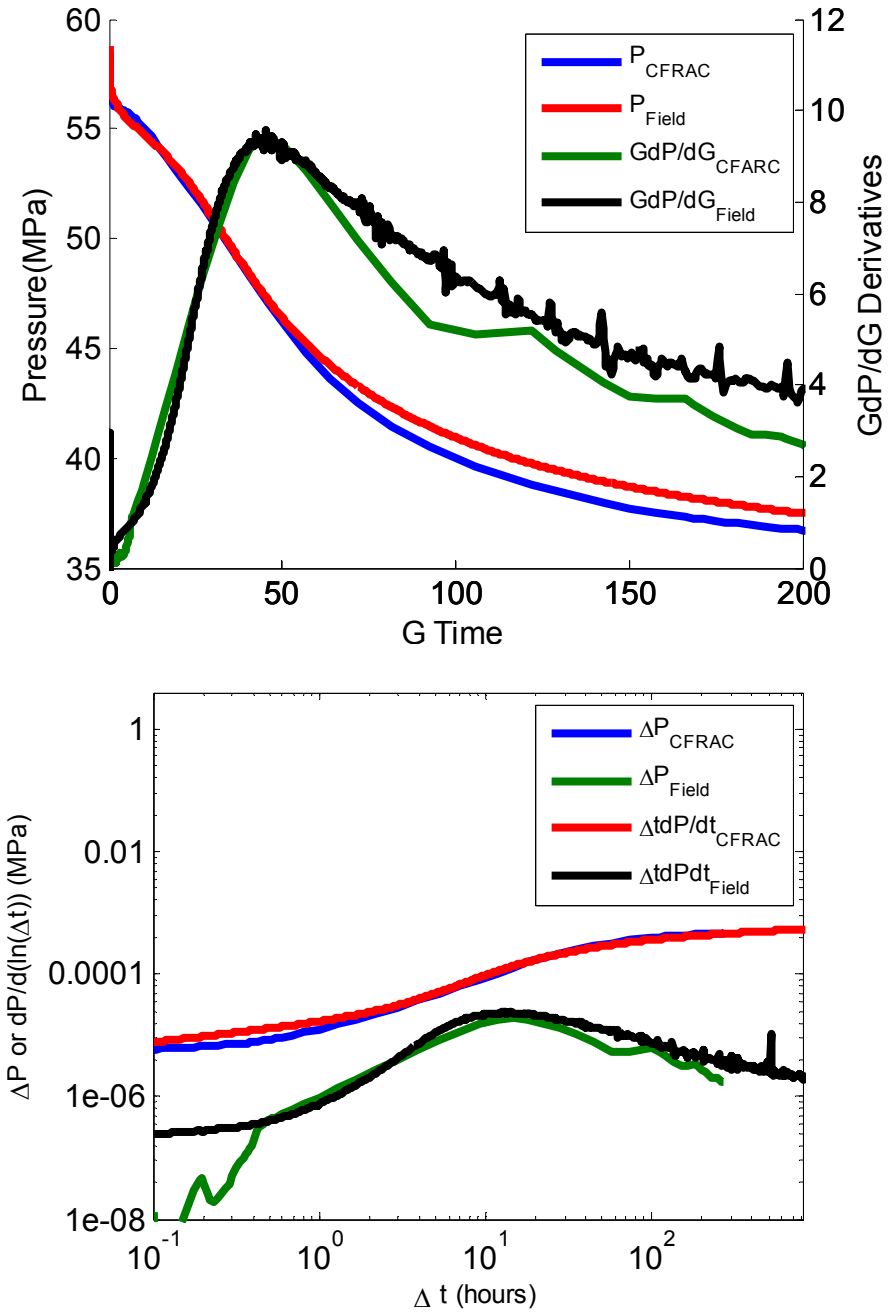

Figure 4.28 G-function analysis and Bourdet log-log analysis plots of multiple strands hydraulic fracture simulation match.

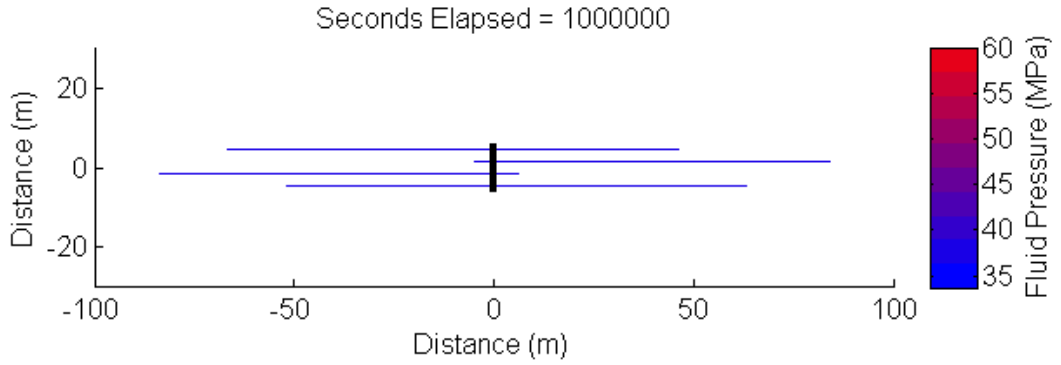

Figure 4.29 Final fracture propagation of the fractures.

4.3.4.3 Transverse fracture opening

For this case, transverse natural fractures are specified orthogonal to the hydraulic fracture. The maximum horizontal stress is specified to be 60 MPa. Therefore, a higher pressure is required to open the transverse fractures than the hydraulic fracture. The leakoff of fluid into the transverse fractures and into the matrix from the transverse fractures, accelerates closure and pressure decay. Figure 4.32 shows that the fracture length is significantly reduced.

Table 4.5 Simulation match input variables for transverse fracture geometry.

Fracture toughness (MPa-m$^{1/2)}$	4
Permeability (nD)	50
Minimum principal stress (MPa)	55.1
90% closure stress (MPa)	50

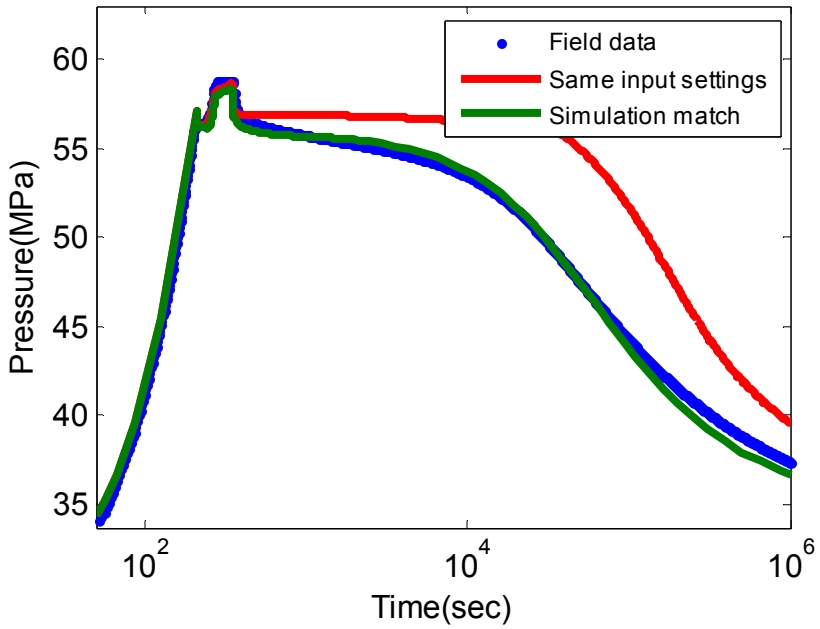

Figure 4.30 Simulation results with transverse fractures.

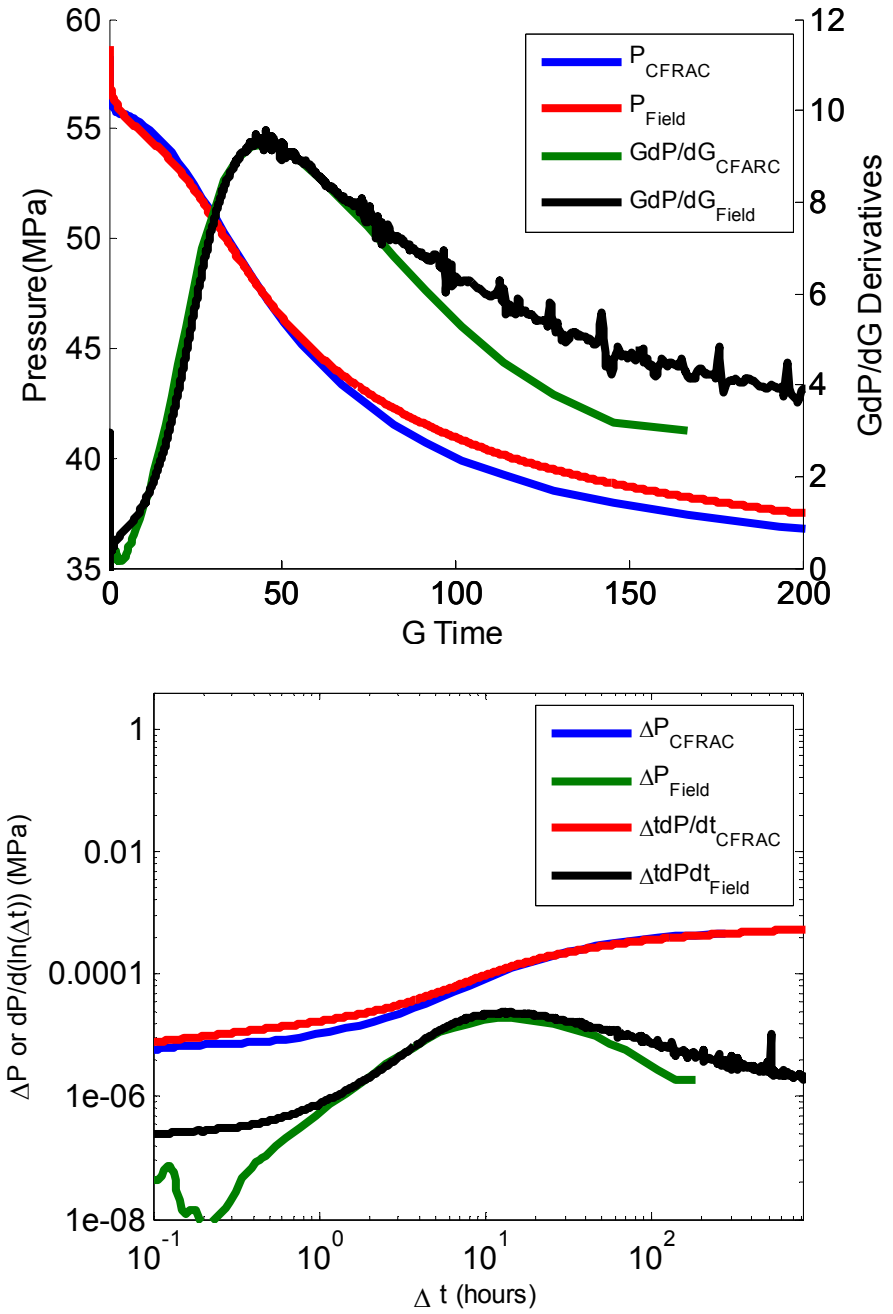

Figure 4.31 G-function analysis and Bordet log-log analysis plots of transverse fractures simulation match.

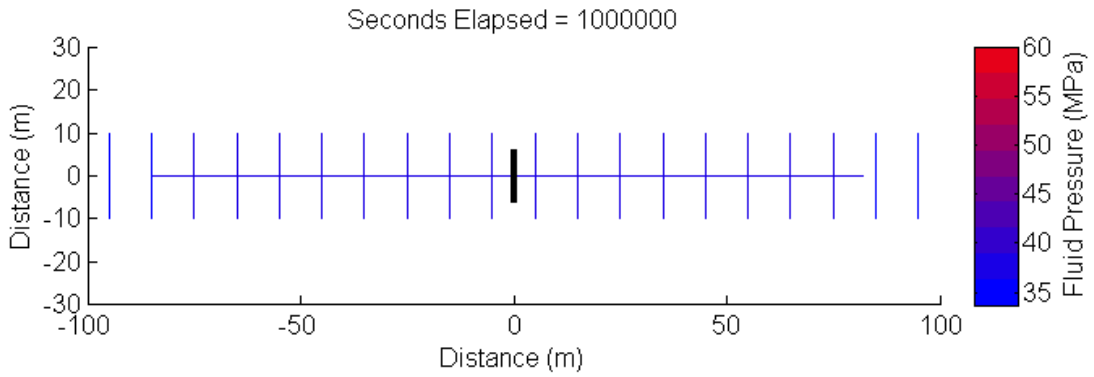

Figure 4.32 Final fracture propagation of the fractures.

Chapter 5: Conclusion

This report investigates methods for picking closure pressure during DFITs. History matching to a field dataset is done with a hydraulic fracturing simulator. Four parameters are analyzed in terms of how those parameters change the pressure transient behavior. Higher fracture toughness shortens the fracture, reducing leakoff, and causing closure to occur later. Higher matrix permeability increases leakoff rate, and causes closure to occur earlier. Higher "90% closure stress" causes higher fracture stiffness, so pressure decreases more abruptly upon closure. Increasing minimum principal stress (holding reservoir fluid pressure constant) increases the pressure prior to closure and increases the rate of leakoff.

An estimate of the minimum principal stress is obtained based on the simulation match, and it is compared with closure pressure estimated by conventional analysis methods such as G-funciton analysis method and Bourdet log-log plot analysis. Based on these results, it appears that the conventional methods underestimate closure pressure.

Fracture compliance can be plotted as a function of time during the simulation. At the moment of fracture closure, the fracture compliance starts to drop. This causes a significant change in the slope of the G*dP/dG curve. Therefore, we propose a new method for picking closure, which is when the G*dP/dG curve begins to sharply deviate upward. Our proposed method picks the closure pressure from the field data, as inferred from the simulation match.

Two nonideal fracture geometries are simulated: four hydraulic fracture strands and transeverse fractures connected to hydraulic fracture. These geometries can also be used to successfully match the field data but give a much shorter fracture length than the simple single planar fracture case.

In the future, additional complex fracture geometries will be examined. Also, our proposed method will be validated with other field datasets.

References

Araujo, O., Lopez-Bonetti, E., Garza, D., & Salinas, G. (2014, May 21). Successful Extended Injection Test for Obtaining Reservoir Data in a Gas-Oil Shale Formation in Mexico. Society of Petroleum Engineers. doi:10.2118/169345-MS

Barree, R. D., Barree, V. L., & Craig, D. (2007, January 1). Holistic Fracture Diagnostics. Society of Petroleum Engineers. doi:10.2118/107877-MS

Barton, N., S. Bandis, & K. Bakhtar. 1985. Strength, deformation and conductivity coupling of rock joints. International Journal of Rock Mechanics and Mining Sciences & Geomechanics Abstracts 22 (3): 121-140, doi: 10.1016/0148-9062(85)93227-9.

Bourdet, Dominique, J. A. Ayoub, Y. M. Pirard. 1989. Use of pressure derivative in well-test interpretation. SPE Formation Evaluation 4 (2): 293-302, doi: 10.2118/12777-PA.

Castillo, J.L. 1987. Modified fracture pressure decline analysis including pressure-dependent leakoff. Paper SPE 164417 presented at the SPE/DOE Low Permeability Reservoir Symposium, Denver, CO, doi: 10.2118/16417-MS.

Cramer, D. D., & D. H. Nguyen. 2013. Diagnostic fracture injection testing tactics in unconventional reservoirs. Paper SPE 163863 presented at the SPE Hydraulic Fracturing Technology Conference, Woodlands, TX, doi: 10.2118/163863-MS.

Economides, M. J., & Nolte, K. G.. 2000. Reservoir Stimulation, 3rd edition. Chichester, England; New York, John Wiley.

Hamid, S., Jackson, B. M., & Legenza, J. E. (1990, January 1). Injection System for Microfrac or Step-Rate Testing. Society of Petroleum Engineers. doi:10.2118/21267-MS

McClure, M. W., & Horne, R. N. (2013, September 30). Characterizing Hydraulic Fracturing With a Tendency for Shear Stimulation Test. Society of Petroleum Engineers. doi:10.2118/166332-MS

McClure, M. W., Christopher A. J. Blyton, Hojung Jung et al. 2014. The effect of changing fracture compliance on pressure transient behavior during diagnostic fracture injection tests. Paper SPE 170956 presented at the SPE Annual Technical Conference and Exhibition, Amsterdam, The Netherlands.

McClure, M., Babazadeh, M., Shiozawa, S., & Huang, J. (2015, February 3). Fully Coupled Hydromechanical Simulation of Hydraulic Fracturing in Three-Dimensional Discrete Fracture Networks. Society of Petroleum Engineers. doi:10.2118/173354-MS

Nolte, K. G. 1979. Determination of fracture parameters from fracturing pressure decline. Paper SPE 8341 presented at the SPE Annual Technical Conference and Exhibition, Las Vegas, Nevada.

Nolte, K. G. 1991. Fracturing-pressure analysis for nonideal behavior. Journal of Petroleum Technology 43 (2): 210-218, doi: 10.2118/20704-PA.

Nordgren, R. P. 1972. Propagation of a vertical hydraulic fracture. Society of Petroleum Engineers Journal 12 (4): 306-314, doi: 10.2118/3009-PA.

Olson, J. E. (2004). Predicting fracture swarms—The influence of subcritical crack growth and the crack-tip process zone on joint spacing in rock.*Geological Society, London, Special Publications*, *231*(1), 73-88.

Olson, J. E. (2007). Fracture aperture, length and pattern geometry development under biaxial loading: a numerical study with applications to natural, cross-jointed systems. Geological Society, London, Special Publications, 289(1), 123-142.

Perkins, T.K. and Kern, L.R. 1961. Widths of Hydraulic Fractures. J Pet Technol 13 (9): 937–949. SPE-89-PA. http://dx.doi.org/10.2118/89-PA.

Proskin, S. A., Scott, J. A., & China, H. S. (1989, January 1). Interpretation of the Minimum Principal Stress From Microfrac Tests. International Society for Rock Mechanics.

Sneddon, I. N. 1946. The distribution of stress in the neighborhood of a crack in an elastic solid. Proceedings of the Royal Society of London Series A 187 (1009): 229-260, doi: 10.1098/rspa.1946.0077

Van Dam, D. B., de Pater, C. J., & Romijn, R. (1998, January 1). Analysis of Hydraulic Fracture Closure in Laboratory Experiments. Society of Petroleum Engineers. doi:10.2118/47380-MS

Vinsome, P. K. W., & Westerveld, J. (1980, July 1). A Simple Method For Predicting Cap And Base Rock Heat Losses In' Thermal Reservoir Simulators. Petroleum Society of Canada. doi:10.2118/80-03-04

Warpinski, N. R., & Teufel, L. W. (1987, February 1). Influence of Geologic Discontinuities on Hydraulic Fracture Propagation (includes associated papers 17011 and 17074). Society of Petroleum Engineers. doi:10.2118/13224-PA

Willis-Richards, J., K. Watanabe, H. Takahashi. 1996. Progress toward a stochastic rock mechanics model of engineered geothermal systems. Journal of Geophysical Research 101 (B8): 17481-17496, doi: 10.1029/96JB00882.

Witherspoon, P. A., J. S. Y. Wang, K. Iwai et al. 1980. Validity of cubic law for fluid flow in a deformable rock fracture. Water Resources Research 16 (6): 1016-1024, doi: 10.1029/WR016i006p01016.

Email: <hjung@utexas.edu >

This report was typed by <Hojung Jung >.